Author/s:
Barria, P;Walsh, KJE;Peel, MC;Karoly, D

Title:
Uncertainties in runoff projections in southwestern Australian catchments using a global climate model with perturbed physics

Date:
2015-10-01

Citation:
Barria, P., Walsh, K. J. E., Peel, M. C. & Karoly, D. (2015). Uncertainties in runoff projections in southwestern Australian catchments using a global climate model with perturbed physics. Journal of Hydrology, 529 (P1), pp.184-199. https://doi.org/10.1016/j.jhydrol.2015.07.040.

Persistent Link:
https://hdl.handle.net/11343/214155

Uncertainties in runoff projections in southwestern Australian catchments using a global climate model with perturbed physics

Pilar Barria[1], Kevin J.E. Walsh[1], Murray C. Peel[2], David Karoly[1]

[1]School of Earth Sciences, University of Melbourne

[2]Department of Infrastructure Engineering, University of Melbourne,

Corresponding author's address: Pilar Barria, School of Earth Sciences, University of Melbourne 3010 Victoria, Australia. E-mail: pbarria@student.unimelb.edu.au

For submission to Journal of Hydrology

May 2015

21 Abstract

22

23 Future projections of water supply under climate change scenarios are fundamental for
24 efficient water resource planning. However, runoff projections are affected by uncertainties
25 in the modelling process that limit their utility to decision makers. The main source of
26 uncertainty in runoff projections are the Global Climate Models (GCMs) used to produce
27 future climate projections. The impact on projected runoff of this uncertainty has mainly
28 been assessed through comparison of multi-model runs of future climate with little
29 exploration of uncertainties inside the models due to different parameterisations. Here we
30 investigate the uncertainty response of projected runoff due to perturbed physics parameter
31 variations within a GCM using a novel 2500 member ensemble from the HadCM3L model.
32 Our research evaluates the uncertainties in runoff modelling for southwest Western
33 Australia, a Mediterranean climate region which has experienced reductions in precipitation
34 during the last decades. Results for future projections in southwest Western Australian
35 catchments indicate reductions in modelled precipitation between 0% to 40% and increases
36 in temperature that fluctuate between 0.5°C and 3°C by 2050- 2080 compared to 1970-
37 2000, which lead to reductions in projected runoff of between 10% and 80%. This range of
38 uncertainty for projected runoff is larger than that calculated for previous estimates of
39 within-model uncertainties of runoff. The perturbed physics approach indicates that current
40 water management assessments underestimate uncertainties in runoff projections.

41

42 Keywords

43 Climate change, water resources, temperature, precipitation.

1. Introduction/Background

Uncertainties in the modelling of the climate system and thus in projections of future changes (Deser et al., 2012; Deser et al., 2014; Hawkins and Sutton, 2009; Hawkins and Sutton, 2011; Kang et al., 2013; Tebaldi and Knutti, 2007) and their impact on hydrology are an active area of research (Peel and Bloschl, 2011; Peel et al., 2015). The Fifth Assessment Report (AR5) of the Intergovernmental Panel on Climate Change (IPCC) (Stocker et al., 2013) includes a review of the main uncertainties in the understanding of the climate system and identified them as crucial in climate change analysis. The IPCC recognized that uncertainties in projections of natural forcing, simulations of clouds in atmosphere-ocean coupled general circulation models (AOGCMs) along with resolution issues in modelling the climate limit the skill of projections on both global and regional scales.

The main source of uncertainties in runoff modelling of future climate arises from the predictions of climate variables (Ardoin-Bardin et al., 2009; Chiew et al., 2009; Chiew et al., 2008; Prudhomme and Davies, 2008a; Xu et al., 2011), such as precipitation and temperature. These uncertainties can be partitioned in three groups: the internal variability of the climate system, the model uncertainty, or uncertainties in the Global Climate Models (GCMs) and the scenario uncertainty (Hawkins and Sutton, 2009; Hawkins and Sutton, 2011). However there are also uncertainties associated with the downscaling and bias correction techniques used to translate the coarse data from the GCM scale to the regional scale of the runoff models, and also in the hydrological model used to simulate runoff.

Quantifying GCM uncertainties is computationally expensive. Currently, two main approaches have been used to assess the uncertainties in GCM analyses: between-GCMs and within-GCMs analysis (Parker, 2013; Peel et al., 2015). The IPCC assessments and the GCMs run in the Coupled Model Intercomparison Project Phase 3 (CMIP3) and Phase 5 (CMIP5; Taylor et al. (2009)) are the main sources of data that researchers have used in multi-model or between-GCMs analyses of uncertainties in climate modelling. An alternative approach employs a "perturbed physics" analysis which explores the impact of parametric uncertainty in climate modelling. This involves using the same model but changing in each simulation a selected set of the parameters that characterize the model physics (Parker, 2013), giving an estimate of the range of possible projections from a single model that might be produced by a plausible range of values of the adjustable parameters within the model. This represents what we define here as "within-GCM" uncertainty when combined with uncertainties due to internal variability and initial conditions. This project uses Climateprediction.net data, which is the largest freely available source of climatic data that explores within-GCM uncertainty using perturbed physics. In the Climateprediction.net experiment the model parameters that represent the atmospheric and ocean physics and the sulphur cycle were perturbed between their minimum and maximum plausible values to obtain an ensemble of different parameter values that were then used to create a large ensemble of model runs (Frame et al., 2009).

Within-GCM uncertainties have so far been assessed through statistical methodologies such as bootstrapping techniques (Prudhomme and Davies, 2008a; Prudhomme and Davies, 2008b), stochastic generation of data (Peel et al., 2015) and hierarchical modelling and Markov chain Monte Carlo simulation techniques (Bastola et al., 2011; Nawaz and

88 Adeloye, 2006). These methodologies involve the generation of multiple replicates of the
89 time series of the climate variables, precipitation and temperature, in which ideally each run
90 has slightly different initial conditions and different trends, all of them physically plausible.

91 So far, hydrological assessments of climate change have mainly explored the impact of
92 between-GCM uncertainties in runoff modelling. In particular in Australia, CMIP3 model
93 results have been directly used to assess changes in water supply in southwest Western
94 Australia (SWA) (Silberstein et al., 2012) and in south- east Australia (Chiew et al., 2009),
95 and concluded that uncertainties between GCMs are large, with a range of results of around
96 30% with respect to the median. Teng et al. (2012) compared runoff projections using
97 CMIP3 and CMIP5 data over Australia showing that uncertainties are very large using both
98 sets of GCM runs, and giving differences of about 50% between the 10th and the 90th
99 percentile of projections.

100 Regarding within-GCM uncertainties, Peel et al. (2015) stochastically replicated
101 precipitation and temperature data from 5 CMIP3 GCM runs 100 times to approximate
102 them for 17 worldwide catchments. The 100 stochastic replicates were passed through a
103 hydrologic model and the standard deviation of the mean annual runoff (MAR) as a
104 percentage of the mean MAR was on average 10.1%, which translates into an uncertainty in
105 MAR of ~20% (2 standard deviations) for each GCM. However, Peel et al. (2015)
106 indicated that their results are likely to underestimate the true within-GCM uncertainty
107 because they only stochastically replicated the noise around the GCM data trend, not the
108 trend itself.

In contrast, perturbed physics experiments allow the generation of simulations of climate variables with different initial conditions and also different trends, all of them physically plausible. To date, there have not been any hydrologic assessments that explore within-GCM uncertainties using the perturbed physics approach. This paper aims to establish the impact on runoff of perturbed physics in a multi-thousand member ensemble of GCM runs with gradually increasing projections of greenhouse gas concentrations (a so-called "transient" experiment). We seek to quantify the true within-GCM uncertainty in runoff projections, used in water availability climate change impact assessments, through the novel approach of using a GCM with perturbed physics. We aim to compare true within-GCM uncertainty from CPDN projections against current approximate statistical approaches or multi-model ensembles. In particular, it is of interest to study these uncertainties in runoff projections in SWA, a region that has already experienced negative trends in precipitation, and where future water resources are endangered (Hennessy et al., 2007).

The IPCC Fifth Assessment Report (AR5) (Stocker et al., 2013) details studies that project significant decreases in precipitation for the period 2081-2100 compared to 1986-2005 in the Mediterranean climate regions of the southern hemisphere; Central Chile, South Africa and SWA (Moss et al. 2008). Current warming trends and future projections of climate variables may impact water resources with important consequences for ecosystems, agricultural and domestic water supply. The present work presents results for southwest Western Australia, due to the current negative trends in precipitation and the projections of drier conditions for this area, however this methodology can be extended to other regions.

1.1 Region of analysis: Southwest Western Australia

SWA is the land area located west of 118°E and south of 32°S (Li et al., 2005), where the majority of Western Australia's population resides (Australian Bureau of Statistics, 2014). According to the Köppen-Geiger Classification (Peel et al., 2007), SWA experiences a temperate, Mediterranean climate with a dry and hot summer and wet winter. Almost 80% of precipitation occurs during May to October. Mean annual rainfall in SWA ranges from 500 mm in the north to 1230 mm in the southern coastal area (Silberstein et al., 2012).

Precipitation in this region is driven by mid-latitude frontal systems associated with the position of the subtropical ridge. This centre of high pressure moves northward (north of SWA) in winter months (after May), and then moves southward during spring months (Charles et al., 2010). In winter months, when the centre of high pressure lies to the north of SWA and the SAM (Southern Annular Mode) is in its negative phase, synoptic features and cold fronts can reach SWA, thus increasing precipitation events. A negative trend in SWA winter precipitation since the mid 1960s has been observed by several researchers (Allan and Haylock, 1993; Ansell et al., 2000; Cai and Cowan, 2006b), while some others identify the shift starting in the mid 1970s (Charles et al., 2010; Frederiksen and Frederiksen, 2007; Hennessy et al., 2007; IOCI, 2012; Petrone et al., 2010; Timbal, 2004). The observed reduction in precipitation after the shift is estimated as being between 10% - 15% (Charles et al., 2010). One of the likely causes of the reduction in precipitation is the positive trend in the SAM (Allan and Haylock, 1993; Cai and Cowan, 2006a; Delworth and Zeng, 2014; IOCI, 2002). Using a K-means algorithm to cluster rainfall patterns, Raut et al. (2014) showed that the positive trend in SAM is linked to the reduction of the frequency of strong fronts in June, and the presence of weak fronts in June-July. These two features account for a half and a third of the total reduction of rainfall in winter months (June-July-

155 August) respectively when the El Niño Southern Oscillation Phenomenon (ENSO) is
156 neutral. Regarding climate change projections, according to Silberstein et al. (2012), based
157 on an ensemble of 15 GCMs, a median decline of 8% in rainfall is projected for SWA by
158 2030 compared to precipitation between 1975 and 2007, which leads to a reduction of 25%
159 in streamflow. Given this background, we have focused our attention on projections of
160 runoff in this region, mainly interested in quantifying how uncertain the projections are
161 when estimated from a GCM with perturbed physics.

162 As climate is a fundamental driver of water availability, the impacts of climate change on
163 water resources and in particular the uncertainties in the projections of runoff are a
164 fundamental area of study. In this paper we present a methodology to analyse uncertainties
165 in runoff modelling using a perturbed physics ensemble from one GCM, which is a novel
166 data set that represents the within-GCM uncertainties. We present a plausible range of
167 runoff projections over three catchments located in SWA, using a multi-thousand ensemble
168 of the GCM with perturbed physics. We compare the results over one catchment analysing
169 within-GCM uncertainties using the stochastic approximation of Peel et al. (2015) and the
170 perturbed physics approach.

171 **2. Data**

172 Three different sources of data are used in this work. First, monthly precipitation and
173 temperature from a GCM with perturbed physics are employed, which gives an ensemble of
174 projected future climates. Second, observed monthly precipitation and temperature
175 measured over Australia are used as input for a hydrologic model. Third, observed monthly

runoff are used to calibrate a hydrologic model. The characteristics of the data are presented in the following subsections.

2.1 GCM with perturbed physics

Data from the Climateprediction.net (CPDN) project (Rowlands et al., 2012) were used for projecting the future climate in the area of study. CPDN provides an ensemble of GCM results with perturbed physics that allows us to explore the within-GCM uncertainties in runoff modelling. The CPDN experiment consists of a GCM run thousands of times with different but realistic perturbations to the parameters of the model's physics, using the personal computers of volunteers. These thousands of simulations were used in this paper to simulate runoff and to analyse the uncertainties associated with perturbed physics in the global climate model.

CPDN uses the HadCM3L GCM, which is a version of the HadCM3 model (Gordon et al., 2000) but with a reduced ocean resolution. The resolution of the model is 2.5° latitude by 3.75° longitude with 19 levels in the vertical in the atmosphere. The ocean resolution has 20 vertical levels and a resolution of 2.5° latitude by 3.75° longitude. The simulations cover the period from 1920 to 2080 (Rowlands et al., 2012).

The CPDN project runs HadCM3L with 10 different versions of the ocean model and 153 different atmospheric parameter configurations, which means 1530 versions of the model with different perturbed physics. The model was spun up for 200 years and subjected to flux adjustment to represent the climate in 1920. Then each individual ensemble was run under control forcing (pre-industrial or representative of 1900 conditions) and transient forcing (time-varying concentrations of greenhouse gases) for the period between 1920 and

198 2080. In this work we used the simulations starting in 1940 as the flux adjustment does not
199 reproduce a stable climate in the first 20 years of simulations (Rowlands et al., 2012). The
200 researchers used both anthropogenic and natural forcing. The anthropogenic forcing
201 corresponds to the A1B scenario (Nakicenovic et al., 2000), which simulate emissions of
202 greenhouse gases and aerosols for a future world of rapid economic growth, assuming that
203 there will be a balance in the use of non- fossil and fossil sources in the energy system,
204 along with an interactive tropospheric sulphur cycle, which through parameterization
205 simulates the radiative effects of sulphate aerosol produced by industrial processes. The
206 natural forcing is represented by changes in solar activity and volcanic eruptions, which are
207 expressed using stratospheric sulphate aerosol.

208 **2.2 Temperature and Precipitation**

209 Gridded monthly observed precipitation and temperature data were used to calibrate the
210 hydrological model used to simulate runoff. The gridded dataset used in this project is the
211 Australian Water Availability Project (AWAP) (Jones et al., 2009). AWAP uses in-situ
212 observations and provides gridded data at a scale resolution of 0.05°x0.05°, which we
213 resampled to a 0.25°x0.25° for our analysis.

214 ARCGIS 9.3 was used to delineate the catchment boundaries using the two-second Shuttle
215 Radar Topography Mission (SRTM) Smoothed Digital Elevation Model (DEM-S) version
216 1.0 (Geoscience Australia, 2010). AWAP data were superimposed over the catchment
217 polygon and area-weighted temperature and precipitation values were calculated for each
218 catchment.

219 **2.3 Runoff data**

Monthly runoff data used to calibrate the hydrological model over southwest Western Australian catchments were taken from the stream gauging sites monitored by the Western Australian government's Department of Water (see the Government of Western Australia, Department of Water, at http://wir.water.wa.gov.au/SitePages/SiteExplorer.aspx).

In order to avoid using runoff data with inconsistencies over time, the runoff monthly time series were checked through the analysis of seasonal variation curves and double mass curves. The latter are scatter plots comparing the cumulative monthly runoff under analysis with cumulative monthly runoff in adjacent catchments. The cumulative monthly runoff was also compared with cumulative monthly precipitation and cumulative monthly temperature from different stations located close to the catchment under study (not shown). When data are consistent, a straight line is expected without jumps or changes in the slope. Through those analyses, we conclude that the observed runoff is consistent over time, and that it can be used to model runoff for climate change assessments.

2.4 Catchments in SWA

The analysis was conducted over three catchments in the area of study (SWA), the Donnelly, Denmark and Helena rivers. The location, catchment area and climatic characteristics of these three catchments are presented in Table 1 and Figure 1.

The Donnelly catchment is a high quality system located in the Warren region of southwest Western Australia. Due to its isolated location, it has not been affected by saline intrusion, and is therefore an important resource for agricultural activities in the region but it also hosts ecosystem refuges (Morgan and Beatty, 2006). Denmark catchment is located in the southeast extreme of the study area, the Great Southern region of Western Australia. The

main land use in the north portion of the catchment is grazing and annual pastures. Currently, salinity issues impede the use of the catchment for supply of drinkable water. Finally, the Helena catchment is located in the northeast of the region, draining the Darling Plateau and passing through the Darling Scarp and the Coastal Plain, where it becomes a tributary of the Swan River which supplies drinking water to the Goldfields region, Kalgoorlie and Perth. These three catchments were selected on the basis of their importance for drinking water supply, support of economic activities in the region and for the ecosystems they host. Differences in precipitation regimes and temperatures were also considered in the selection process. The Helena River is the driest catchment with 665 mm of observed mean annual precipitation. The Donnelly River is the wettest catchment with 1004 mm of observed mean annual precipitation, while the Denmark catchment has 835 mm of annual precipitation.

3. Methodology

We follow a three stage methodology often used in projections of water resources research, but here introduce the novel approach of assessing the impact of perturbed physics on runoff projections, and comparing against results obtained from previous methods developed in this field. First, the perturbed physics GCM data are evaluated over the region of study. Second, a bias correction to the GCM data is applied to scale the GCM data and match each observed catchment data, and finally a calibrated hydrological model is used to simulate runoff for the future using the GCM precipitation and temperature data.

3.1 Evaluation of CPDN output

263 We evaluated the ability of the CPDN data to represent the climate of SWA, first
264 comparing the raw precipitation and temperature with observed data. Then, we compared
265 the relation between ENSO and SAM with precipitation and temperature using observed
266 datasets and the CPDN data in order to evaluate whether the CPDN model output data
267 represent the relation between the main drivers of climate in the region and the variables in
268 the study.

269 The CPDN data were released in "Giorgi regions", based on the regions analysed by Giorgi
270 et al. (2001) that include both land and sea. Thus to compare land-based AWAP
271 precipitation and air temperature at 1.5 metres to CPDN data required the application of
272 correction factors. The procedure consisted of calculating a scale factor that represents the
273 difference between the air temperature at a height of 1.5 metres from HadCRUT3v (Brohan
274 et al., 2006; Jones, 1994) over the same spatial extent as the CPDN Giorgi region (which
275 include land and sea), and the HadCRUT3v temperature over just the land in this region.
276 This factor was calculated and applied seasonally to the AWAP data. The scaled AWAP
277 temperature data were then compared to the CPDN ensemble. Monthly gridded
278 precipitation data from the Global Precipitation Climatology Project (Adler et al., 2003)
279 were used to calculate similar scaling factors for precipitation to account for the difference
280 in precipitation in the CPDN Giorgi region and precipitation over just land. The scaled
281 AWAP precipitation was then compared to the CPDN data.

282 ENSO (El Niño Southern Oscillation) and SAM are the main drivers of precipitation and
283 temperature variability in Australia (Arblaster et al., 2011; Hendon et al., 2013). In SWA it
284 is of particular interest for evaluating the relation between SAM and precipitation, because
285 of the influence the SAM has had on reductions in rainfall (Raut et al., 2014). The

Climateprediction.net dataset was evaluated to determine its skill in simulating large scale circulation patterns and their relationship with local variables over the area of study. Three correlation coefficients (Kendall, Spearman and Pearson) were used to analyse the relation between the variables in this region and circulation patterns over the observed period (1940-2000).

The Southern Annular Mode is defined as the difference in the normalized zonal average mean sea level pressure between 40°S and 65°S. Gong and Wang [1999] developed an Index that measures SAM, the regional Antarctic Oscillation Index, detailed in Equation 1.

$$AOIR_t = \frac{MSLP_{40°S}(t) - \overline{MSLP_{40°S}(t)}}{\sigma_{MSLP\ 40°S}(season)} - \frac{MSLP_{65°S}(t) - \overline{MSLP_{65°S}(t)}}{\sigma_{MSLP\ 65°S}(season)} \quad (1)$$

Where AOIRt is the Antarctic Oscillation Index for month t, MSLP40°S is the mean sea level pressure (MSLP) at 40°S averaged over all longitudes, MSLP65°S is the MSLP at 65°S averaged over all longitudes, $\overline{\mathrm{MSLP}_{40°\mathrm{S}}(\mathrm{t})}$ is the MSLP at 40°S averaged over all longitudes and the whole period of time under analysis for month t, $\overline{\mathrm{MSLP}_{65°\mathrm{S}}(\mathrm{t})}$ is the MSLP at 65°S averaged over all longitudes and the whole period of time under analysis for month t, $\sigma_{\mathrm{MSLP}\ 40°\mathrm{S}}(\mathrm{season})$ is the standard deviation of MSLP at 40°S averaged over all longitudes for a particular season, and $\sigma_{\mathrm{MSLP}\ 65°\mathrm{S}}(\mathrm{season})$ is the standard deviation of MSLP at 65°S averaged over all longitudes for a particular season.

We used an approximation to the AOIR index in this paper, in order to fit the Giorgi regions in which CPDN data were released. The approximation consists of replacing the $\mathrm{MSLP}_{40°\mathrm{S}}(\mathrm{t})$ by the MSLP averaged over all SWA (-38°S to -28°S, 110°E- 125°E) and $\mathrm{MSLP}_{65°\mathrm{S}}(\mathrm{t})$ by the MSLP over the Antarctic region (-90°S to -55°S, 0°e to 360° E).

306 The index used to represent ENSO variability is the Niño 3.4 index, which was calculated
307 following the methodology described by NCAR (2013). The first stage was computing the
308 total area averaged SST from the Niño 3.4 region (5°N-5°S, 120°-170°W). Then the
309 anomalies were calculated by subtracting the monthly mean SST for the period 1950 to
310 1979 from the data. Finally the series were smoothed with a 3-month running mean.
311 Anomalies higher/lower than 0.5°C/-0.5°C are defined as El Niño and La Niña
312 respectively.

313 **3.2 Bias Correction Methodology**

314 GCM data have a different spatial scale (hundreds of kilometres) to the catchment scale and
315 generally require downscaling and bias correction. In this project a Quantile-Quantile
316 methodology (Themeßl et al., 2011), which is a type of statistical downscaling method, is
317 used. The procedure is based on matching the empirical cumulative distribution functions
318 of the GCM simulations to the empirical cumulative distribution function of the
319 observations. This is a direct method because the predictor and the predictand are the same
320 variable (temperature or precipitation) and has the advantage of being parameter-free
321 because the empirical cumulative distribution is matched for each variable. Themeßl et al.
322 (2011) described the methodology of correction using the following equations for the
323 calibration period (in this case the period in which observed runoff data are available for
324 each catchment), which in this project will be applied on a monthly basis for each
325 catchment:

$$Y_{t,catchment}^{cor} = X_{t,catchment}^{raw} + CF_{t,catchment} \quad (2)$$

$$CF_{t,catchment} = ecdf_{moy,catchment}^{obs,cal-1}\left(P_{t,catchment}\right) - ecdf_{moy,catchment}^{mod,cal-1}\left(P_{t,catchment}\right) \quad (3)$$

$$P_{t,catchment} = ecdf^{mod,cal}_{moy,catchment}\left(X^{raw}_{t,catchment}\right) \quad (4)$$

Where $Y^{cor}_{t,catchment}$ is the bias corrected (*cor*) GCM variable over the catchment under study for month *t*, $X^{raw}_{t,catchment}$ is the raw GCM variable over the catchment under study for month *t*, $CF_{t,catchment}$ is the correction factor calculated during the calibration period for month *t*, $ecdf^{mod,cal}_{moy,catchment}$ is the empirical cumulative distribution function for the GCM variable in a particular month of the year (*moy*) for the calibration period (*cal*), and $ecdf^{obs,cal}_{moy,catchment}$ is the empirical cumulative distribution function for the observed variable in a particular *moy* for the calibration period.

The difference between the inverse ecdf ($ecdf^{-1}$) of the simulation and the observation over the calibration period for every probability represents the bias correction. An example is presented in Figure 2, in which each grey line represents the inverse ecdf for one of the 2500 CPDN simulations of precipitation for December (1920-2000) and the red line represents the inverse ecdf of observed AWAP precipitation for December (1920-2000). The red arrow represents the correction for one simulation, which is the difference between the simulated and observed inverse ecdfs for that particular probability. For future projections, the same correction factors are applied to every simulation, matching the simulated values of the variable for the projection with the calibration period. For new extremes in the modelled period (values that have not been observed during the calibration period), higher or lower than observations, the correction factor of the highest or the lowest observed value is applied respectively.

3.3 Perm Model Description

346 The hydrological model used in this work is PERM (Peel et al., 2015). A schematic
347 diagram of the model structure is presented in Figure 3. This is a lumped conceptual
348 monthly model that uses as input monthly precipitation and temperature data observed or
349 modelled over the catchment. PERM has five model parameters that require calibration: the
350 rate of snowmelt and potential evapotranspiration (**ETrate**, mm/°C/month); the proportion
351 of snowmelt volume to runoff (**Melt**); the soil moisture storage capacity (**Smax**, mm); the
352 baseflow linear recession parameter (**K**); and the interception storage capacity (**Imax**, mm).
353 The model considers three main stores: the vegetation interception store (IC), the soil
354 moisture store (SMS) and the snow store (ACCUM). When temperature is > 0°C then all
355 precipitation enters the interception store. Once the maximum capacity (Imax) is reached
356 any remaining precipitation becomes throughfall (TFall) to the soil moisture store. Snow
357 only accumulates when temperature is ≤ 0°C and the snow begins to melt once temperature
358 rises > 0°C. Melting snow either becomes runoff (SnowF) or infiltrates (SMI) into the soil
359 moisture store. Runoff is calculated through a volume balance and considers snow flow,
360 partial area flow (PAreaF), soil moisture excess flow (SMF), once the soil moisture store
361 reaches it maximum value (Smax), and base flow (BF). Evaporation from the interception
362 store (AET_{INT}) and soil moisture store (AET_{SOIL}) are calculated as a linear function of
363 temperature and water availability. In this analysis, snow does not occur in the three
364 catchments being modelled, which effectively reduces PERM to a four parameter model as
365 the **Melt** parameter becomes redundant due to ACCUM being zero. An automatic pattern
366 search optimization method was used to calibrate the five model parameters (see Peel et al.,
367 2015 for details). Ten different parameter sets were used as starting points to increase the
368 likelihood of finding the global optimum of parameter values. The calibration sought to
369 minimise the objective function defined as the sum of squared differences between the

estimated and observed annual runoff. Although the model is run on a monthly time step, it will be used to simulate annual runoff for future climates. Therefore, penalties were applied to the objective function (OBJ) in order to ensure that the calibrated model reproduces summary statistics of observed annual runoff.

Peel et al. (2015) summaries these penalties as:

If the estimated and observed mean annual runoff differ by;

- More than 5% then OBJ = OBJ x 5
- More than 10% then OBJ = OBJ x 25
- More than 20% then OBJ = OBJ x 125

If the estimated and observed annual coefficient of variation differ by;

- More than 5% then OBJ = OBJ x 5
- More than 10% then OBJ = OBJ x 25
- More than 20% then OBJ = OBJ x 125

The evaluation method used for the model is a K-Fold cross-validation (Efron and Tibshirani, 1993), with K=3. The entire time series is divided in three groups, two of them are used to calibrate and the third one to evaluate the model performance. This process is repeated 3 times until all thirds have been used to evaluate model performance. The metrics used to evaluate model performance are the Nash & Sutcliffe Efficiency value (Nash and Sutcliffe, 1970), which compares observed and modelled annual runoff, and the annual R^2 (square of the correlation coefficient) between observed runoff and modelled runoff. Details of the calibration methodology can be found in Peel et al. (2015).

4. Results

392 Modelled and observed temperature, precipitation and runoff for the three catchments under
393 study are presented in this section. First we evaluate the ability of un-bias corrected CPDN
394 data to simulate the climate of the study region during the observed period. Then, we
395 investigate how uncertainties in precipitation and temperature from CPDN translate into
396 uncertainties in runoff projections for the next decades. Finally, the perturbed physics
397 results are compared against an approximation based on stochastic generation of data.

398 **4.1 Evaluation of CPDN data**

399 Seasonal and annual raw (not bias corrected) precipitation and temperature simulated by the
400 CPDN project were compared to scaled observed AWAP data in order to assess how these
401 GCM runs simulate SWA climate. The scale factor was introduced to make the observed
402 data, which has been measured over land only, consistent with the raw CPDN data that
403 includes both land and ocean. After incorporating the scale factor a good agreement
404 between observed and modelled data was observed for annual and seasonal climate
405 variables. The annual values are presented in Figure 4 for precipitation and Figure 6 for
406 temperature. In these figures, we plot in grey all the CPDN simulations of annual
407 precipitation and temperature for the period between 1940 and 2080, including in blue the
408 median of the simulations and the 5 and 95 percentiles. The red line shows the observed
409 AWAP annual precipitation and temperature between 1940 and 2000. In Figure 5 and
410 Figure 7, we show histograms of annual medians and standard deviations of precipitation
411 and temperature respectively simulated by CPDN between 1940 and 2000 (the observed
412 period) and the annual median and standard deviation obtained from AWAP data. In terms
413 of temperature the annual median of the CPDN simulations for the observed period (1940-
414 2000) underestimates by 0.23°C the observed annual median of temperature during the

415 same period. Substantial differences are observed in the annual standard deviation over the
416 same period, with CPDN underestimating annual standard deviation of temperature by
417 0.14°C relative to the observed value (see the results presented in Table 3). In terms of
418 precipitation we found that the annual median of CPDN simulations between 1940 and
419 2000 differs by 6.2% from the observed data, and the CPDN annual standard deviation
420 underestimates the observed value by 45%, (Table 4).

421 In Figure 4 the median of the CPDN simulations of annual precipitation is similar to the
422 median value of the scaled observed (AWAP) annual precipitation, and the median of the
423 simulations reproduce the reductions in observed precipitation since mid 1960s (Allan and
424 Haylock, 1993; Ansell et al., 2000; Cai and Cowan, 2006b). Results presented in Figure 6
425 indicate that the median of the CPDN simulations of annual temperature approximately fits
426 the scaled observed annual temperature, and that the median of the simulations is consistent
427 with the positive trend in scaled observed temperature. From these results we conclude that
428 CPDN is better at reproducing annual temperature over SWA than annual precipitation, and
429 that the medians of the climate variables are better simulated than the variability, measured
430 by the standard deviation. Prior to the hydrologic modelling we resolve these differences
431 using the bias correction methodology described in section 3.2.

432 In order to evaluate whether the CPDN data represent the relation between the main drivers
433 of climate in the region, we compared the relation between ENSO and SAM with
434 precipitation and temperature using observed data and CPDN data. ENSO is one of the
435 main drivers of rainfall in Australia (Allan, 1988; Nicholls et al., 1997; Wang and Hendon,
436 2007). Nicholls et al. (1997) indicated that the relation between ENSO and rainfall over
437 Australia shows a considerable multi-decadal variability, driving wet and dry periods in its

438 different phases (El Niño and La Niña). However, the main area of influence of ENSO in
439 terms of precipitation is north and eastern Australia (Nicholls and Lavery, 1992; Risbey et
440 al., 2009), with no significant influence over SWA, since SAM is the main driver of
441 precipitation in that zone (Raut et al., 2014). ENSO inter-decadal variability has been also
442 found to be associated with variations in surface temperature in Australia (Power et al.,
443 1999a; Power et al., 1999b). Power et al. (1999a) found a correlation of 0.1 between annual
444 temperature and SOI (Southern Oscillation Index) when the Inter-decadal Pacific
445 Oscillation (IPO) is over the threshold of 0.5. Therefore, we just explored the correlation
446 between annual and winter precipitation and SAM, and annual temperature and ENSO.
447 The median of the correlation coefficients between SAM and annual and winter
448 precipitation obtained using three different methodologies (Spearman, Kendall and Pearson
449 correlation) for all the CPDN simulations are presented in Table 2. These correlations are
450 statistically significant at the 95% level. The mean correlation between annual SAM and
451 annual precipitation, considering all the statistical significant simulations and three
452 methodologies, is -0.3, while for winter SAM and winter precipitation it is -0.52. We also
453 calculated correlations between the SAM index as defined by Nan and Li (2003) and annual
454 and winter observed precipitation (AWAP) considering Pearson, Kendall and Spearman
455 correlation coefficients. The correlation between observed winter precipitation and winter
456 SAM is statistically significant at -0.39. These results are presented in Table 2. The
457 influence of SAM on SWA precipitation is greatest in the winter season as this is the period
458 in which precipitation is mostly concentrated in this region. The medians of statistical
459 significant correlation coefficients, for the three methodologies, between annual ENSO and
460 annual temperature in SWA are presented in Table 2. The mean of the three medians is

461 0.26, which is larger than the correlation of 0.16 (not statistically significant) obtained from
462 the observed NIÑO 3.4 Index and AWAP data.

463 Our results indicate that CPDN reproduces the observed negative correlation between
464 annual precipitation, winter precipitation and SAM, which is the main driver of the changes
465 in precipitation during the last decades. After this analysis we conclude that CPDN
466 represents appropriately the climate of SWA, and is suitable for studying the uncertainties
467 in future projections in this region.

468 **4.2 Runoff Modelling**

469 The PERM model was calibrated for each catchment using observed area-weighted
470 temperature and rainfall from the AWAP data as input to PERM for the period in which
471 observed runoff data are available.
472 For the Donnelly River at Strickland, 32 years of observed runoff data in the period 1961-
473 1992 were used to calibrate the model. Twenty eight years of observed runoff were used for
474 modelling the Helena River at Ngangaguringuring, which corresponds to the period
475 between 1973 and 2000 and finally 40 years of observed runoff were available in the
476 Denmark River at Kompup, which corresponds to the period between 1961 and 2000.
477 PERM is run on a monthly time step, however we assess model performance during
478 calibration and evaluation on an annual basis. In the following analyses the majority of
479 runoff results presented are for annual data with some seasonal data. Therefore, our
480 evaluation of PERM's performance at annual intervals is consistent with our later analysis.
481 The calibrated parameters and the performance of the model for every catchment is given in
482 Table 5, the coefficient of determination (R^2) and the annual Nash & Sutcliffe coefficient of

efficiency (N&SE) represent the evaluation of the model skill in simulating runoff in the catchments, where a value of 1 in each of them means a perfect match. The model was evaluated using a K-Fold cross-validation with K=3 (Efron and Tibshirani, 1993), where the evaluation N&SE was calculated from the 2 thirds not used to calibrate the model. Results of the model performance during calibration and evaluation are presented in Table 5 and Table 6 respectively. We found good model performance during calibration and evaluation for the Donnelly River at Strickland and the Denmark River at Kompup, but poorer performance for the Helena River at Ngangaguringuring. Despite this poorer performance we decided to include the Helena river in our analysis because it is an important catchment, one of the tributaries that supply water to Perth and because it is a dry catchment, thus more susceptible to climate change impacts.

The calibrated model was then run 2500 times using the bias corrected precipitation and temperature data from CPDN to simulate runoff from 2000 to 2080 under the A1B scenario in each catchment in SWA. When performing the bias correction methodology we found that for precipitation the ecdf of monthly future simulations of winter CPDN is drier or is shifted to less precipitation than the ecdf of precipitation during the observed period. The main difference lies in the extreme lower quantile, where the ecdf of precipitation of future simulations presents a shift to lower precipitation than the observed and in some cases to higher extremes as well. For temperature the ecdf of monthly temperature shows a shift to higher temperatures with higher hot extremes. The CPDN precipitation and temperature monthly ecdfs for the observed and future (2000-2080) periods are available in Figure S1 of the Supplementary material.

After introducing the bias correction we found that the difference between the medians of the simulated temperatures (CPDN) and the observed annual temperature (AWAP) for the

507 period between 1961 and 1992 (which corresponds to the period in which observed runoff
508 data are available in Donnelly catchment) is 0.02 °C. The difference in the standard
509 deviation of the CPDN simulations of annual temperature and observed annual temperature
510 (AWAP) is 0.01°C, much lower than the 0.14°C difference for the raw series. For
511 precipitation the differences for the same period are 0.79% and 3.7% for median and
512 standard deviation respectively, improving considerably the 6.2% and 45% obtained from
513 raw data. See this information in Table 3 and Table 4.
514 Bias corrected annual precipitation and temperature CPDN simulations were compared
515 against observed data (the AWAP weighted average) for each catchment, with the results
516 for Donnelly catchment presented in Figure 8 (precipitation) and Figure 9 (temperature).
517 The bias corrected methodology was applied to the complete period of record, but the
518 correction was developed only over the period of observed runoff data available in each
519 catchment, which in Figures 8 and 9 corresponds to the period between 1961 and 1992. In
520 these figures, grey lines correspond to the 2500 bias corrected simulations from CPDN,
521 blue lines are the median, 5 and 95 percentiles of the data and the red line the AWAP
522 observations. In both cases a good graphical agreement between the observed data (red
523 line) and the median of the CPDN data (blue line) was obtained for the period in which the
524 bias correction was developed (period in which runoff data were available).
525 According to Figure 9, positive trends for temperature in Donnelly River at Strickland have
526 been seen during the observed period (1940-2000) and faster increases are shown in the
527 later period (2000-2080), which can be noticed from the blue lines that represent the
528 median and the 5 and 95 percentiles. This result was also observed in Helena and Denmark
529 catchments for annual and for seasonal results. Conversely, negative trends in annual
530 precipitation are shown (Figure 8) during the observed period (1940-2000) and faster

531 decreases are expected for the later period (2000-2080) for Donnelly catchment, which can
532 be seen from the blue lines that represent the median and percentiles of the simulations.
533 These results were also observed in Helena and Denmark rivers (not shown). The decrease
534 in precipitation is concentrated in the winter season, with changes in summer precipitation
535 being almost negligible (not shown), which is in agreement with the literature (Alexander et
536 al., 2007; Charles et al., 2010; Nicholls and Lavery, 1992).

537 We show the annual runoff simulations using the CPDN climate data in Figure 10. Similar
538 results were obtained for the other two catchments so we present the figures for Donnelly
539 catchment only. From Figure 10, negative trends in Donnelly at Strickland runoff are
540 observed in the projections for the period 2000-2080, concordant with the trends in
541 precipitation, the main driver of runoff in the area. This result was also observed in the
542 Helena River at Ngangaguringuring and Denmark River at Kompup. The projections of
543 annual precipitation, annual runoff, seasonal precipitation and seasonal runoff were
544 computed for the period 2050-2080 and compared to 1970-2000 for all catchments, then we
545 computed histograms including all the simulations. The histograms for seasonal differences
546 in the Donnelly catchment are presented in Figure 11. Since similar results were obtained
547 for the other two catchments, just results for Donnelly River at Strickland are shown.

548 Decreases in precipitation with a median of around 20% are projected for precipitation in
549 winter, spring and autumn, which leads to decreases in runoff of around 50% for winter and
550 autumn. The response of spring runoff to reduced precipitation is larger than the other
551 seasons, which might be driven in part by reduced catchment wetness at the beginning of
552 spring following reduced precipitation in autumn and winter and for the increases in
553 temperature and potential evapotranspiration during these months. Summer precipitation

554 shows no real change but has a large spread of results, which is explained due to the
555 summer rainfall in these catchments being negligible. A large spread in the projections of
556 runoff is also observed, with a median decrease of around 50%, which is caused by the
557 combination of reduced precipitation in most seasons and higher temperatures in all
558 seasons.

559 Histograms of annual runoff and rainfall difference for the three catchments are presented
560 in Figure 12. In all catchments a reduction in annual precipitation with a median of around
561 20% is expected, which leads a reduction in runoff of more than double (~50%). The
562 Helena catchment, which is the driest catchment among the three, is the most sensitive to
563 changes in precipitation, with a median reduction in runoff of around 65%, driven by a
564 reduction in rainfall with a median of around 20%. The results indicate that the drier the
565 catchment, the more sensitive the response in runoff to changes in precipitation and the
566 larger the spread of the projections, which is consistent with the understanding of runoff
567 sensitivity to changes in precipitation increasing as the humidity ratio decreases (Dooge,
568 1992; Dooge et al., 1999; Sankarasubramanian et al., 2001).

569 **4.3 Comparison of within-GCM uncertainties from stochastic generation of data**

570 Here we present a comparison of results from a GCM with perturbed physics to that from
571 the stochastic generation of GCM data in order to identify any differences in the
572 quantification of uncertainties in precipitation and runoff modelling for the Donnelly
573 catchment. The GCM perturbed physics results from the previous section are shown in box-
574 plot form (Figure 13) for annual precipitation and runoff over the Donnelly catchment.
575 Stochastic generation results are drawn from Peel et al. (2015), where monthly precipitation

576 and temperature data from 5 GCMs, selected for their good performance in simulating
577 observed climate (McMahon et al., 2015), were stochastically replicated 100 times each.
578 The stochastic methodology of Peel et al. (2015) is to de-trend the GCM data, replicate the
579 de-trended data (both the signal and the noise around the trend) and add the trend to the
580 stochastic data to form the stochastic replicate of the GCM run. Thus each stochastic
581 replicate for a given GCM has the same trend but different stochastic data around the trend.
582 Peel et al. (2015) indicated that they expected their stochastic method to under-estimate the
583 true within-GCM uncertainty due to not replicating the trend. Results in Figure 13 indicate
584 that the range of uncertainty using perturbed physics is larger than that using stochastic
585 generation of data. The boxplots present the range of different simulations of rainfall and
586 runoff, where the 25th and 75th percentiles are represented in the box, and the 97.5th and
587 2.5th percentiles in the lines. Considering the differences between the 75th and the 25th
588 percentiles as a percentage of the median, a 12% range in precipitation for the 2035-2064
589 period is obtained using stochastic generation, compared to a 22% range using CPDN data
590 for the same period. These results are amplified when analysing runoff: a range of 28% of
591 the median runoff modelled for the period between 2035 and 2064 using stochastic
592 generation is considerably smaller than the 57% range for the same variable and the same
593 period using perturbed physics GCM data.

594 **4.4 Comparison of within-GCM uncertainties from GCM perturbed physics**

595 As our main interest is quantifying uncertainties in water projections due to within-GCM
596 uncertainties we have mostly focused on the whole range of plausible projections rather
597 than the spread of results caused by a single parameter. However, we also explored single

598 parameter uncertainties relative to the entire CPDN ensemble for a few parameters that we
599 identified as important for the simulation of precipitation.

600 Regarding uncertainties in input forcing in the GCM, Rowlands et al. (2012) presented an
601 analysis of the main drivers of uncertainties in the CPDN simulations. They performed a
602 linear variance decomposition of all the CPDN ensemble grouping the physical parameters
603 into three groups. Solar, volcanic and sulphur cycle parameters were grouped as forcing
604 parameters, with climate sensitivity used as a proxy for atmospheric physics and vertical
605 diffusivity as representative of ocean physics. Their results showed that the atmospheric
606 physics parameterizations accounted for most of the uncertainty among the ensemble (50%
607 during the last 20 years), followed by uncertainties in forcing and in last position the ocean
608 parameters. This was explained as due to the longer time-scale responses of oceans in the
609 climate system.

610 As an exploratory analysis we calculated the histograms of the differences in runoff for the
611 periods between 2050-2080 and 1970-2000 for the different plausible values of five
612 parameters: *rhcrit* (critical relative humidity for cloud formation), *cw_land* (threshold cloud
613 water content for rain over land), *eacf* (large-scale cloud coverage when the specific
614 humidity in the grid box is equal to the saturation value), *ct* (accretion constant – time
615 constant for conversion of cloud droplets to rain) and *vf1* (cloud ice fall speed). All
616 parameters were selected for their importance in the GCM parameterization of rainfall,
617 which is the main driver of runoff in SWA.

618 In Figure 14 we present histograms of change in mean annual runoff obtained by selecting
619 different values of the parameter *rhcrit*, which shows the spread of runoff change and the

620 median change relative to the whole ensemble of CPDN. Figures for the other parameters
621 are contained in the Supplementary information. The histograms in Figure 14 show the
622 whole ensemble of simulations in blue (2500) and the simulations using each one of the
623 different *rhcrit* values in grey. We also plotted the median of the whole ensemble (red line)
624 and the median of the group of simulations obtained using an *rhcrit* value (red dotted line).
625 The three different values of *rhcrit* produce results with differences in median of 9%. The
626 median of the reductions in runoff for the lowest *rhcrit* is -46%, and for the highest *rhcrit* is
627 -55%. The spread of simulations moves to higher reductions in runoff when *rhcrit* is larger.
628 This is due to the importance of *rhcrit* for cloud formation – as *rhcrit* increases cloud
629 formation becomes harder, which results in less precipitation and less runoff. Among all the
630 parameters analysed, *rhcrit* produced the largest impact on runoff reductions, showing how
631 important parameterisations of cloud formation are for projections of climate and runoff.

632 **5. Discussion and Conclusions**

633 In this paper we have studied how uncertainties in the parameters specified within-GCM
634 physics parameterisations translates into uncertainties in runoff projections. Our results
635 show that uncertainties in projections of runoff, precipitation and temperature for the second
636 half of this century using perturbed physics in a single GCM are very large. Uncertainties in
637 GCM parameterisations in precipitation and temperature translate into even larger
638 uncertainties in runoff projections (approximately doubled), with a hydrological sensitivity
639 of around 2.5, which is consistent with the values calculated by Chiew (2006) and Jones et
640 al. (2006). It is important to emphasize that these uncertainties correspond just to
641 uncertainties within a single GCM, without considering uncertainties in emissions scenario,
642 downscaling/bias correction, hydrological modelling or vegetation response to CO_2

643 enrichment. However, due to the large number of perturbations and initial conditions
644 explored in the CPDN data, it is possible that these simulations match some simulations
645 produced by other GCMs, covering between-GCM uncertainties as well. The impact on
646 runoff of within-GCM uncertainty due to perturbed physics has not previously been
647 analysed, so these results are useful to compare with studies that assess only multi-model
648 uncertainties.

649 In this study, plausible projections in annual precipitation indicate a reduction between the
650 years 2050-2080 compared to 1970-2000 that range between 0% and 40% for the Donnelly
651 and Denmark Rivers and between 0% and 50% for the drier Helena catchment. The range of
652 projected decrement in annual precipitation drives a runoff decrement between 10% and
653 80% over the same period, and this reduction is also larger in the Helena catchment (0%-
654 90%). A reduction of around 22% in annual and winter precipitation leads to a descrease of
655 50% in runoff which is a larger reduction than that found using stochastic generation of
656 data, as an approach for assessing within-GCM uncertainties.

657 Winter reductions in precipitation and runoff for every catchment are very similar to the
658 annual changes, mainly because around 80% of annual precipitation falls in winter months
659 in these catchments. Summer and spring runoffs are most sensitive to changes in
660 precipitation due to increases in temperature during these months and the drier conditions in
661 the catchment resulting from the reduced autumn and winter rainfall, which increase
662 sensitivity to changes in precipitation, as reported by Chiew (2006).

663 According to the results shown in this paper, the CPDN projects reductions in precipitation
664 for the period 2050-2080 in all the catchments, and the hydrological model results indicate

665 larger reductions in runoff for the same period for the three catchments. However some
666 differences between catchments were observed. The driest catchments are more sensitive to
667 changes in precipitation: for example, the Helena River in which the change in modelled
668 runoff is more than double the change in precipitation. This is concordant with the results
669 presented by Dooge et al. (1999) and Sankarasubramanian et al. (2001) which indicated that
670 the drier the catchment the more sensitive the runoff to changes in precipitation. The Helena
671 River result is very important as it is representative of the area around Perth, the largest city
672 in Western Australia, and these reductions would have a significant impact on surface water
673 resources available for water supplies.

674 The perturbed physics GCM results showed that uncertainties, quantified as the range
675 between 25th and the 75th percentiles in the histogram of plausible projections using CPDN
676 data, are approximately double those from stochastic generation of GCM data. This
677 confirms that the stochastic approximation of within-GCM uncertainty of Peel et al (2015)
678 underestimates true within-GCM uncertainty as expected. In both cases the range of
679 projections for runoff is larger, more than double the range in precipitation projections,
680 indicating the sensitivity of runoff to precipitation.

681 The difference between the 10th and 90th percentiles of modelled annual runoff for the
682 period between 2046-2065, compared to 1961-2000, using CPDN data averaged over the
683 three catchments is around 78%, which is much larger than the 50% obtained by Teng et al.
684 (2012) using the GCM ensembles runs available in CMIP3 and CMIP5 for Australian
685 catchments.

686 Considering the analysis of uncertainties due to the variation of single parameters in the
687 GCM physics parameterizations, we found that of the five atmospheric parameters
688 investigated the parameter representing critical relative humidity for cloud formation
689 produced the largest changes in terms of precipitation and runoff. *Rhcrit* produced
690 reductions in the median of runoff projections that fluctuated between -46% and -55%,
691 indicating the importance of this parameter to cloud formation processes in the GCM.
692 As we said before, our work present some limitations. First of all the GCM output is
693 available in a monthly basis, then we bias corrected the data for every catchment monthly,
694 but we did not consider the biases in other time scales and among multiple variables.
695 Recent work from Mehrotra and Sharma (2015) indicates that by bias correcting the
696 climatic variables in a joint structure and considering different time scales (daily, monthly
697 and seasonally) better results are observed in the representation of persistence properties
698 and distributions of the variables. Second, we calibrated a lumped hydrological model
699 which does not consider vegetation response to CO2 enrichment, and then we assume that
700 the catchments will present the same soil and vegetation conditions in the future, not
701 considering changes and influences of vegetation which could result in an underestimation
702 of uncertainties. Still, CPDN data with its limitations is a powerful tool for understanding
703 and studying the impacts of parameterizations in a GCM in climatic and runoff projections,
704 reaching the main aim of our study satisfactorily.
705 Finally, the results from the perturbed physics approach indicate that current studies of
706 future runoff under climate change, which solely consider between-GCM variability, tend to
707 underestimate the uncertainty in runoff. The methodology presented here can be extended to
708 other catchments located in other regions, and future work in central Chilean catchments is
709 planned as part of this project.

6. Acknowledgements

The research was funded, in part, by the Australian Research Council (ARC) Centre of Excellence for Climate System Science (grant CE110001028) and ARC research grant FT120100130. Additional funds were provided by scholarship Becas Chile.

We would like to express our gratitude to UK-based University of Oxford, Rutherford Appleton Laboratory and Open University for providing the GCM data, which can be accessed from the website of the project *http://www.climateprediction.net*. We are also grateful to the Australian Water Availability Project for providing the observed hydrometeorological data used in this work, which can be accessed from the website *http://www.csiro.au/awap*. We also thank the two anonymous reviewers whose comments helped improve the manuscript.

7. References

Australia Bureau of Statistics, 2014. 3218.0 - Regional Population Growth, Australia, 2012-13. <http://www.abs.gov.au/Ausstats/abs@.nsf/mf/3218.0> (accessed 06.11.2014).

Adler, R.F. et al., 2003. The version-2 global precipitation climatology project (GPCP) monthly precipitation analysis (1979-present). J. Hydrometeorol., 4(6): 1147-1167. http://dx.doi.org/10.1175/1525-7541(2003)004<1147:TVGPCP>2.0.CO;2.

Alexander, L., Hope, P., Collins, D., Trewin, B., 2007. Trends in Australia's climate means and extremes: a global context. Aust. Meteorol. Mag., 56: 1-18.

Allan, R.J., 1988. El Niño southern oscillation influences in the Australasian region. Prog. Phys. Geog., 12(3): 313-348.

Allan, R.J., Haylock, M.R., 1993. Circulation features associated with the winter rainfall decrease in southwestern Australia. J. Clim., 6(7): 1356-1367. http://dx.doi.org/10.1175/1520-0442(1993)006<1356:CFAWTW>2.0.CO;2.

Ansell, T., Reason, C., Smith, I., Keay, K., 2000. Evidence for decadal variability in southern Australian rainfall and relationships with regional pressure and sea surface temperature. Int. J. Climatol., 20(10): 1113-1129. http://dx.doi.org/10.1002/1097-0088(200008)20:10<1113::AID-JOC531>3.0.CO;2-N.

Arblaster, J.M., Meehl, G.A., Karoly, D.J., 2011. Future climate change in the Southern Hemisphere: Competing effects of ozone and greenhouse gases. Geophys. Res. Lett., 38(2). http://dx.doi.org/10.1029/2010gl045384.

Ardoin-Bardin, S. et al., 2009. Using general circulation model outputs to assess impacts of climate change on runoff for large hydrological catchments in West Africa. Hydrol. Sci. J., 54(1): 77-89. http://dx.doi.org/10.1623/hysj.54.1.77.

Bastola, S., Murphy, C., Sweeney, J., 2011. The role of hydrological modelling uncertainties in climate change impact assessments of Irish river catchments. Adv. Water Resour., 34(5): 562-576. http://dx.doi.org/10.1234/12345678.

Brohan, P., Kennedy, J.J., Harris, I., Tett, S.F.B., Jones, P.D., 2006. Uncertainty estimates in regional and global observed temperature changes: A new data set from 1850. J. Geophys. Res., 111: 2156-2202. http://dx.doi.org/10.1029/2005JD006548.

Cai, W., Cowan, T., 2006a. SAM and regional rainfall in IPCC AR4 models: Can anthropogenic forcing account for southwest Western Australian winter rainfall reduction?. Geophys. Res. Lett., 33(24). http://dx.doi.org/10.1029/2006gl028037.

Cai, W., Cowan, T., 2006b. SAM and regional rainfall in IPCC AR4 models: Can anthropogenic forcing account for southwest Western Australian winter rainfall reduction?. Geophys. Res. Lett., 33(24): 1-5. http://dx.doi.org/10.1029/2006gl028037.

Charles, S. et al., 2010. Climate analyses for south-west Western Australia. A report to the Australian Government from the CSIRO South-West Western Australia Sustainable Yields Project. CSIRO, Australia, 10.1007/s10584-007-9390-9. http://dx.doi.org/10.1007/s10584-007-9390-9.

Chiew, F., Teng, J., Vaze, J., Kirono, D., 2009. Influence of global climate model selection on runoff impact assessment. J. Hydrol., 379(1-2): 172-180. http://dx.doi.org/10.1016/j.jhydrol.2009.10.004.

Chiew, F. et al., 2008. Modelling Runoff and Climate Change Impact on Runoff in 178 Catchments in the Murray-Darling Basin Using Sacramento and SIMHYD Rainfall-Runoff Models. Proceedings of Water Down Under 2008, 2008: 10.

767 Chiew, F.H.S., 2006. Estimation of rainfall elasticity of streamflow in Australia. Hydrol. Sci. J., 51(4):
768 613-625. http://dx.doi.org/10.1623/hysj.51.4.613.
769 Delworth, T., Zeng, F., 2014. Regional rainfall decline in Australia attributed to anthropogenic
770 greenhouse gases and ozone levels. Nat. Geosci., 7: 583-587.
771 http://dx.doi.org/10.1038/ngeo2201.
772 Deser, C., Phillips, A., Bourdette, V., Teng, H., 2012. Uncertainty in climate change projections: the
773 role of internal variability. Clim. Dyn., 38(3-4): 527-546. http://dx.doi.org/10.1007/s00382-
774 010-0977-x.
775 Deser, C., Phillips, A.S., Alexander, M.A., Smoliak, B.V., 2014. Projecting North American Climate
776 over the Next 50 Years: Uncertainty due to Internal Variability*. J. Clim., 27(6): 2271-2296.
777 http://dx.doi.org/10.1175/jcli-d-13-00451.1.
778 Dooge, J.C., 1992. Sensitivity of runoff to climate change: A Hortonian Approach

779 Bulletin American Meteorological Society, 73(12).
780 Dooge, J.C., Bruen, M., Parmentier, B., 1999. A simple model for estimating the sensitivity of
781 runoff to long-term changes in precipitation without a change in vegetation. Adv. Water
782 Resour., 23: 153-163.
783 Efron, B., Tibshirani, R.J., 1993. An introduction to the bootstrap, vol. 57 of Monographs on
784 Statistics and Applied Probability. New York: Chapman and Hall.
785 Frame, D.J. et al., 2009. The climateprediction.net BBC climate change experiment: design of the
786 coupled model ensemble. Philos Trans A Math Phys Eng Sci, 367(1890): 855-70.
787 http://dx.doi.org/10.1098/rsta.2008.0240.
788 Frederiksen, J.S., Frederiksen, C.S., 2007. Interdecadal changes in southern hemisphere winter
789 storm track modes. Tellus A, 59(5): 599-617. http://dx.doi.org/10.1111/j.1600-
790 0870.2007.00264.x.
791 Geoscience Australia, 2010. Digital Elevation Models. User Guide 1. Second DSM, DEM & DEM-S 3
792 second DSM, DEM & DEM-S Version 1.0.3. Sales & Distribution Geoscience Australia.
793 Giorgi, F. et al., 2001. Emerging patterns of simulated regional climatic changes for the 21st
794 century due to anthropogenic forcings. Geophys. Res. Lett., 28(17): 3317-3320.
795 http://dx.doi.org/10.1029/2001gl013150.
796 Gordon, C. et al., 2000. The simulation of SST, sea ice extents and ocean heat transports in a
797 version of the Hadley Centre coupled model without flux adjustments. Clim. Dyn., 16(2-3):
798 147-168. http://dx.doi.org/10.1007/s003820050010.
799 Hawkins, E., Sutton, R., 2009. The potential to narrow uncertainty in regional climate predictions.
800 Bull. Am. Meteorol. Soc., 90(8): 1095-1107. http://dx.doi.org/10.1175/2009BAMS2607.1.
801 Hawkins, E., Sutton, R., 2011. The potential to narrow uncertainty in projections of regional
802 precipitation change. Clim. Dyn., 37(1-2): 407-418. http://dx.doi.org/10.1007/s00382-010-
803 0810-6
804 Hendon, H.H., Lim, E.-P., Arblaster, J.M., Anderson, D.L.T., 2013. Causes and predictability of the
805 record wet east Australian spring 2010. Clim. Dyn., 10.1007/s00382-013-1700-5.
806 http://dx.doi.org/10.1007/s00382-013-1700-5.
807 Hennessy, K. et al., 2007. Australia and New Zealand. In 'Climate Change 2007: Impacts,
808 Adaptation and Vulnerability. Contribution of Working Group II to the Fourth Assessment
809 Report of the Intergovernmental Panel on Climate Change. Cambridge University Press:
810 Cambridge, UK: 507-540.
811 IOCI, 2002. Climate variability and change in south west Western Australia. IOCI Panel: 34.
812 IOCI, 2012. Western Australia's Weather and Climate: A Synthesis of Indian Ocean Climate
813 Initiative Stage 3 Research. CSIRO and BoM, Australia: 117.

814 Jones, D.A., Wang, W., Fawcett, R., 2009. High-quality spatial climate data-sets for Australia.
815 Australian Meteorological and Oceanographic Journal, 58: 233.
816 http://dx.doi.org/10.1.1.222.6311.
817 Jones, P.D., 1994. Hemispheric surface air temperature variations: a reanalysis and an update to
818 1993. J. Clim., 7(11): 1794-1802. http://dx.doi.org/10.1175/1520-
819 0442(1994)007<1794:HSATVA>2.0.CO;2.
820 Jones, R.N., Chiew, F.H.S., Boughton, W.C., Zhang, L., 2006. Estimating the sensitivity of mean
821 annual runoff to climate change using selected hydrological models. Adv. Water Resour.,
822 29(10): 1419-1429. http://dx.doi.org/10.1016/j.advwatres.2005.11.001.
823 Kang, S.M., Deser, C., Polvani, L.M., 2013. Uncertainty in Climate Change Projections of the Hadley
824 Circulation: The Role of Internal Variability. J. Clim., 26(19): 7541-7554.
825 http://dx.doi.org/10.1175/jcli-d-12-00788.1.
826 Li, Y., Cai, W., Campbell, E.P., 2005. Statistical Modeling of Extreme Rainfall in Southwest Western
827 Australia. J. Clim., 18: 12.
828 McMahon, T.A., Peel, M.C., Karoly, D.J., 2015. Assessment of precipitation and temperature data
829 from CMIP3 global climate models for hydrologic simulation. Hydrol. Earth Syst. Sci., 19(1):
830 361-377. http://dx.doi.org/10.5194/hess-19-361-2015.
831 Mehrotra, R., Sharma, A., 2015. Correcting for systematic biases in multiple raw GCM variables
832 across a range of timescales. J. Hydrol., 520: 10.
833 Morgan, D., Beatty, S., 2006. Fish fauna of the Donnelly River, Western Australia. Freshwater Fish
834 Research, Murdoch University report to the Southern Forests Landcare: 106.
835 Nakicenovic, N. et al., 2000. Special report on emissions scenarios: a special report of Working
836 Group III of the Intergovernmental Panel on Climate Change. Pacific Northwest National
837 Laboratory, Richland, WA (US), Environmental Molecular Sciences Laboratory (US).
838 Nan, S., Li, J., 2003. The relationship between the summer precipitation in the Yangtze River valley
839 and the boreal spring Southern Hemisphere annular mode. Geophys. Res. Lett., 30(24).
840 Nash, J., Sutcliffe, J.V., 1970. River flow forecasting through conceptual models part I—A
841 discussion of principles. J. Hydrol., 10(3): 282-290 http://dx.doi.org/10.1007/s10584-005-
842 9043-9.
843 Nawaz, N., Adeloye, A., 2006. Monte Carlo assessment of sampling uncertainty of climate change
844 impacts on water resources yield in Yorkshire, England. Clim. Change, 78(2-4): 257-292.
845 http://dx.doi.org/10.1007/s10584-005-9043-9.
846 Nicholls, N., Drosdowsky, W., Lavery, B., 1997. Australian rainfall variability and change. Weather,
847 52(3): 66-72.
848 Nicholls, N., Lavery, B., 1992. Australian rainfall trends during the twentieth century. Int. J.
849 Climatol., 12(2): 153-163. http://dx.doi.org/10.1002/joc.3370120204.
850 Parker, W.S., 2013. Ensemble modeling, uncertainty and robust predictions. Wiley Interdisciplinary
851 Reviews: Climate Change, 4(3): 213-223 http://dx.doi.org/10.1002/wcc.220.
852 Peel, M.C., Bloschl, G., 2011. Hydrological modelling in a changing world. Prog. Phys. Geog., 35(2):
853 249-261. http://dx.doi.org/10.1177/0309133311402550.
854 Peel, M.C., Finlayson, B.L., McMahon, T.A., 2007. Updated world map of the Köppen-Geiger
855 climate classification. Hydrol. Earth Syst. Sci. Discuss., 4: 439–473.
856 http://dx.doi.org/10.5194/hess-11-1633-2007
857 Peel, M.C., Srikanthan, R., McMahon, T.A., Karoly, D.J., 2015. Approximating uncertainty of annual
858 runoff and reservoir yield using stochastic replicates of global climate model data. Hydrol.
859 Earth Syst. Sci., 19(4): 1615-1639. http://dx.doi.org/10.5194/hess-19-1615-2015.

Petrone, K.C., Hughes, J.D., Van Niel, T.G., Silberstein, R.P., 2010. Streamflow decline in southwestern Australia, 1950-2008. Geophys. Res. Lett., 37(11). http://dx.doi.org/10.1029/2010gl043102.

Power, S., Casey, T., Folland, C., Colman, A., Mehta, V., 1999a. Inter-decadal modulation of the impact of ENSO on Australia. Clim. Dyn., 15(5): 319-324.

Power, S. et al., 1999b. Decadal climate variability in Australia during the twentieth century. Int. J. Climatol., 19(2): 169-184.

Prudhomme, C., Davies, H., 2008a. Assessing uncertainties in climate change impact analyses on the river flow regimes in the UK. Part 1: baseline climate. Clim. Change, 93(1-2): 177-195. http://dx.doi.org/10.1007/s10584-008-9464-3.

Prudhomme, C., Davies, H., 2008b. Assessing uncertainties in climate change impact analyses on the river flow regimes in the UK. Part 2: future climate. Clim. Change, 93(1-2): 197-222. http://dx.doi.org/10.1007/s10584-008-9461-6.

Raut, B.A., Jakob, C., Reeder, M.J., 2014. Rainfall Changes over Southwestern Australia and Their Relationship to the Southern Annular Mode and ENSO. J. Clim., 27(15): 5801-5814. http://dx.doi.org/10.1175/jcli-d-13-00773.1.

Risbey, J.S., Pook, M.J., McIntosh, P.C., Wheeler, M.C., Hendon, H.H., 2009. On the Remote Drivers of Rainfall Variability in Australia. Monthly Weather Review, 137(10): 3233-3253. http://dx.doi.org/10.1175/2009mwr2861.1.

Rowlands, D.J. et al., 2012. Broad range of 2050 warming from an observationally constrained large climate model ensemble. Nat. Geosci., 5(4): 256-260. http://dx.doi.org/10.1038/ngeo1430.

Sankarasubramanian, A., Vogel, R.M., Limbrunner, J.F., 2001. Climate elasticity of streamflow in the United States. Water Resour. Res., 37(6): 1771-1781. http://dx.doi.org/10.1029/2000wr900330.

Silberstein, R.P. et al., 2012. Climate change and runoff in south-western Australia. J. Hydrol., 475: 441-455. http://dx.doi.org/10.1016/j.jhydrol.2012.02.009.

Stocker, T.F. et al., 2013. Technical Summary. In: Climate Change 2013: The Physical Science Basis. Contribution of Working Group I to the Fifth Assessment Report of the Intergovernmental Panel on Climate Change.

Taylor, K.E., Stouffer, R.J., Meehl, G.A., 2009. A summary of the CMIP5 experiment design. WCRP.

Tebaldi, C., Knutti, R., 2007. The use of the multi-model ensemble in probabilistic climate projections. Philos Trans A Math Phys Eng Sci, 365(1857): 2053-75. http://dx.doi.org/10.1098/rsta.2007.2076.

Teng, J., Chiew, F., Vaze, J., 2012. Will CMIP5 GCMs reduce uncertainty in hydrological projections?, AGU Fall Meeting Abstracts, pp. 1435.

Themeßl, M.J., Gobiet, A., Heinrich, G., 2011. Empirical-statistical downscaling and error correction of regional climate models and its impact on the climate change signal. Clim. Change, 112: 449-468. http://dx.doi.org/10.1007/s10584-011-0224-4.

Timbal, B., 2004. Southwest Australia past and future rainfall trends. Climate Research, 26(3): 233-249.

Wang, G., Hendon, H.H., 2007. Sensitivity of Australian rainfall to inter-El Nino variations. J. Clim., 20(16): 4211-4226.

Xu, H., Taylor, R.G., Xu, Y., 2011. Quantifying uncertainty in the impacts of climate change on river discharge in sub-catchments of the Yangtze and Yellow River Basins, China. Hydrol. Earth Syst. Sci., 15(1): 333-344. http://dx.doi.org/10.5194/hess-15-333-2011.

907 **List of tables and Figures**

926 Figure 5 Histogram of median of simulated (CPDN) annual precipitation (mm) for the
927 period between 1940 and 2000. Comparison of median of observed data (AWAP), as
928 indicated with the open star, and the median of all the simulations during the same period,
929 indicated with an asterisk

930 Figure 6 Comparison of raw CPDN annual temperature and scaled AWAP annual
931 temperature for SWA. Grey lines represent the 2500 simulations of temperature from
932 CPDN. 95^{th}, 5th percentiles and median of the simulations are presented as blue lines and
933 AWAP annual temperature is plotted with a red line

934 Figure 7 Histogram of the median of simulated (CPDN) annual temperature (°C) for the
935 period between 1940 and 2000. Comparison of median of observed data (AWAP) as
936 indicated with the open star and the median of all the simulations during the same period,
937 indicated by an asterisk

938 Figure 8 Bias corrected annual precipitation over Donnelly River at Strickland (with respect
939 to observed period 1961-1992). Grey lines represent the 2500 simulations of bias corrected
940 precipitation from CPDN project. 95th, 5th percentiles and median of the simulations are
941 presented as blue lines and AWAP annual precipitation is plotted with a red line. The bias
942 correction was developed over the observed period 1961-1992

943 Figure 9 Bias corrected annual temperature over Donnelly River at Strickland. Grey lines
944 represent the 2500 simulations of bias corrected temperature from CPDN project. 95th, 5th
945 percentiles and median of the simulations are presented as blue lines and AWAP annual
946 temperature is plotted with red line. The bias correction was developed over the observed
947 period 1961-1992

948 Figure 10 Simulated annual runoff over Donnelly River at Strickland. Grey lines represent
949 the 2500 simulations of runoff using PERM model run with bias corrected precipitation and
950 temperature from CPDN. 95th, 5th percentiles and median of the simulations are presented
951 as blue lines and observed runoff is plotted with a red line

952 Figure 11 Histograms of seasonal changes in precipitation and runoff over Donnelly River
953 at Strickland

954 Figure 12 Histograms of annual changes in precipitation and runoff in all of the catchments

955 Figure 13 Boxplot of uncertainties in precipitation and runoff using CPDN data and
956 stochastic generation, in the Donnelly River at Strickland for the period 2035 - 2064

957 Figure 14 Histograms of annual changes in runoff considering all the simulations of CPDN
958 and the groups of simulations with different perturbations of the parameter *rhcrit*. Red line
959 represents the median of the whole ensemble and dotted red line the median of the
960 simulations for a particular perturbation of *rhcrit*

961

962 **Table 1** Catchment location, area, and mean annual precipitation and temperature

River Station	Latitude (°)	Longitude (°)	Area km^2	Precipitation mm	Temperature °C
Helena River at Ngangaguringuring	-31.94	116.4	327	665	17
Donnelly River at Strickland	-34.33	115.77	780	1004	15.2
Denmark River at Kompup	-34.87	117.32	502.4	835	15.3

963

964 **Table 2** Correlation coefficients between Southern Annular Mode, ENSO, precipitation and
965 temperature observed and simulated by CPDN

	CPDN annual precipitation - SAM	CPDN winter precipitation - SAM	CPDN annual temperature - ENSO	Observed Annual precipitation - SAM	Observed winter precipitation - SAM	Observed annual temperature - ENSO
Spearman	-0.33	-0.57	0.3	-0.30	-0.46	0.17
Kendall	-0.23	-0.4	0.21	-0.19	-0.31	0.12
Pearson	-0.34	-0.6	0.27	-0.27	-0.41	0.18

966

967 Table 3 Differences in median and standard deviation of AWAP temperature and CPDN
968 temperature

	Median AWAP data (°C)	Median CPDN (°C)	Dif Median (°C)	Standard dev. AWAP data (°C)	Standard dev. CPDN data (°C)	Dif. Standard Dev. (°C)
Raw Temperature over SWA	16.09	15.86	-0.23	0.45	0.31	-0.14
Bias corrected Temperature over Donnelly River at Strickland	15.20	15.18	-0.02	0.42	0.43	+0.01

969

970 **Table 4** Differences in median and standard deviation of AWAP precipitation and CPDN
971 precipitation

	Median AWAP data (mm)	Median CPDN (mm)	Dif Median (%)	Standard dev. AWAP data (mm)	Standard dev. CPDN data (mm)	Dif. Standard Dev. (%)
Raw Precipitation over SWA	429.24	402.69	6.19	100.33	54.58	45.60
Bias corrected Precipitation over Donnelly River at Strickland	1003.9	995.93	0.79	150.46	156.02	3.70

972

973 **Table 5** PERM calibration results

	Parameters					Evaluation Annual Modelled and Observed Runoff	
Catchment	Smax	ETrate	K	Melt	Imax	R^2	N&SE
Helena River at Ngangaguringuring	200	60	0.41	0.02	100	0.62	0.59
Donnelly River at Strickland	767.81	7.56	0	0.27	23.88	0.94	0.94
Denmark River at Kompup	936.56	12.22	0.27	0.83	92.75	0.78	0.78

974

975

976 **Table 6** PERM evaluation results

Catchment	Annual N&SE	Obs. MAR (mm)	Mod. MAR (mm)	Dif Obs. And Mod. MAR (%)	Obs Cv	Mod. Cv	Dif Obs. And Mod. Cv (%)
Helena River at Ngangaguringuring	0.60	6.41	6.10	4.93	0.89	0.88	0.84
Donnelly River at Strickland	0.92	162.72	162.98	0.16	0.43	0.41	5.00
Denmark River at Kompup	0.70	58.93	57.92	1.70	0.58	0.56	4.83

977

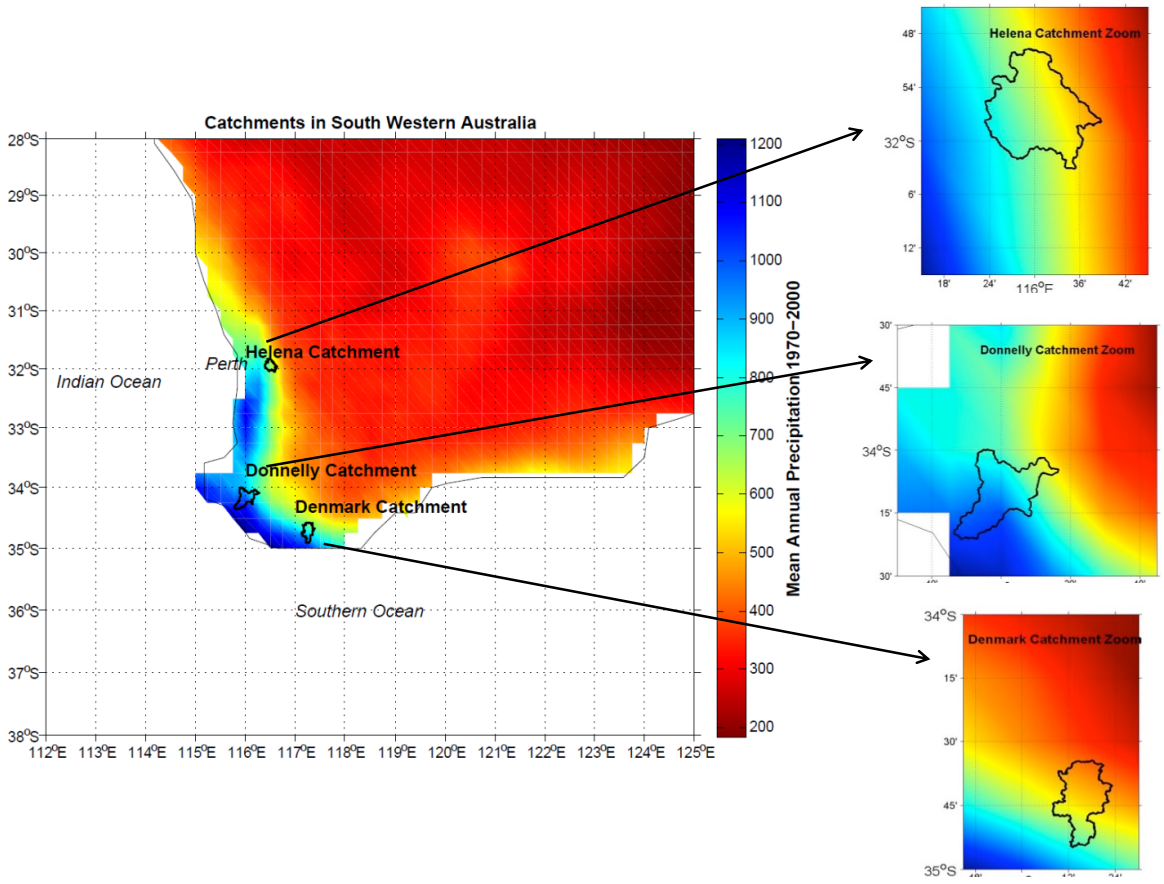

978

979 **Figure 1** Location of the catchments in southwest Western Australia, along with mean

980 annual rainfall (1970-2000)

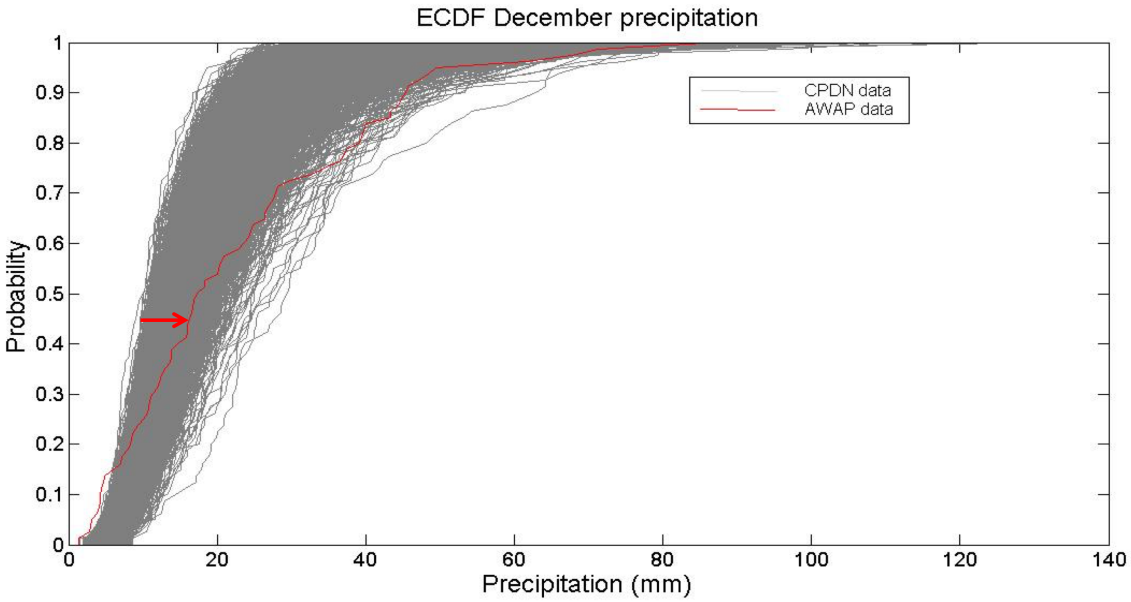

981

982 **Figure 2** Bias correction methodology for precipitation in Donnelly River at Strickland

983 during December

984

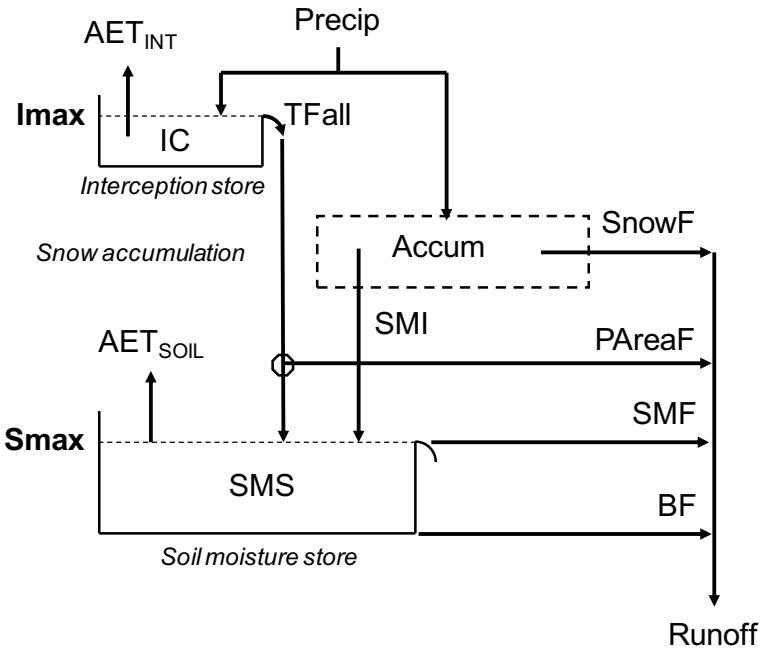

985

986 **Figure 3** PERM model scheme

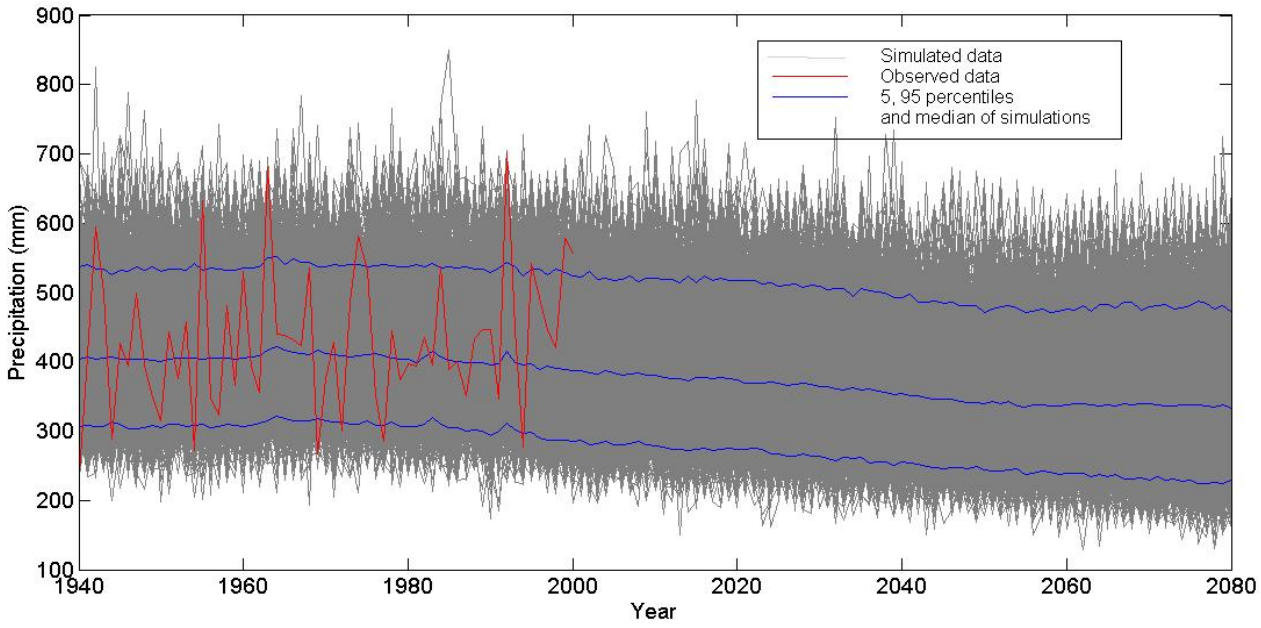

987

988 **Figure 4** Comparison of raw CPDN annual precipitation and scaled AWAP annual

989 precipitation for SWA. Grey lines represent the 2500 simulations of precipitation from

990 CPDN. 95th, 5th percentiles and median of the simulations are presented as blue lines and

991 AWAP annual precipitation is plotted with a red line

992

993

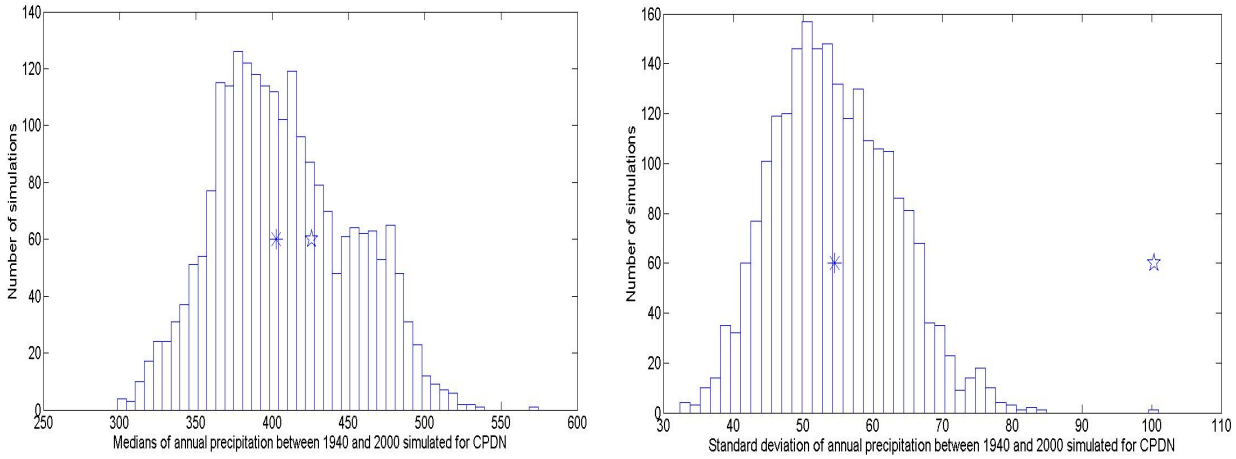

994 **Figure 5** Histogram of median of simulated (CPDN) annual precipitation (mm) for the
995 period between 1940 and 2000. Comparison of median of observed data (AWAP), as
996 indicated with the open star, and the median of all the simulations during the same period,
997 indicated with an asterisk

998

999

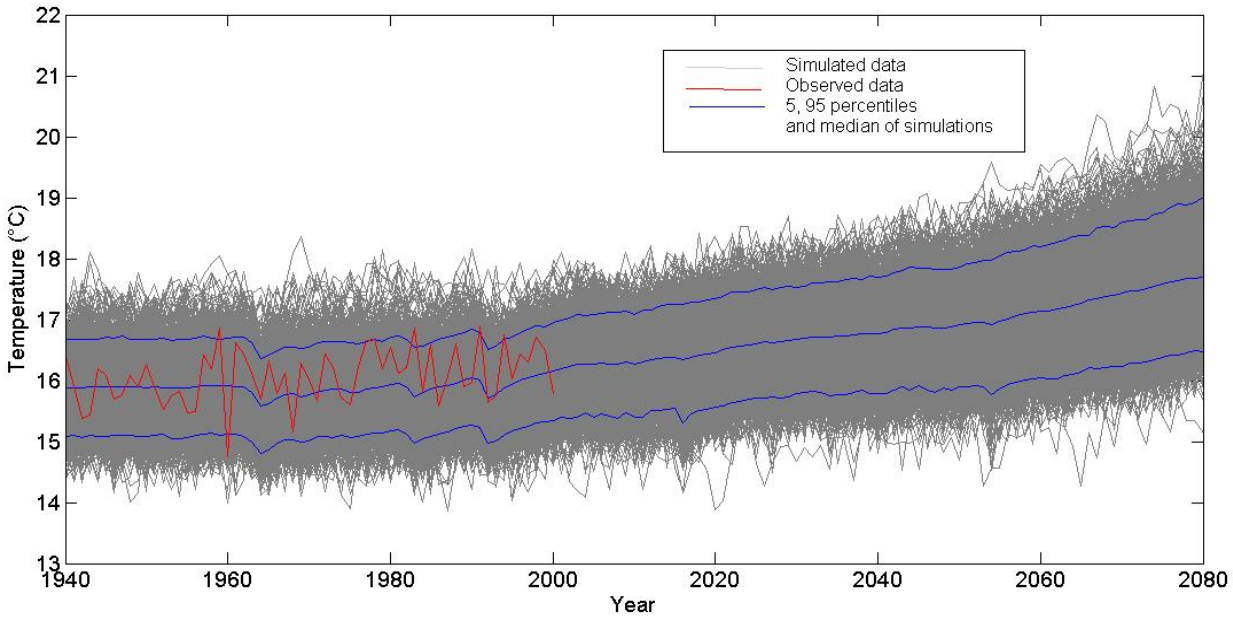

Figure 6 Comparison of raw CPDN annual temperature and scaled AWAP annual temperature for SWA. Grey lines represent the 2500 simulations of temperature from CPDN. 95th, 5th percentiles and median of the simulations are presented as blue lines and AWAP annual temperature is plotted with a red line

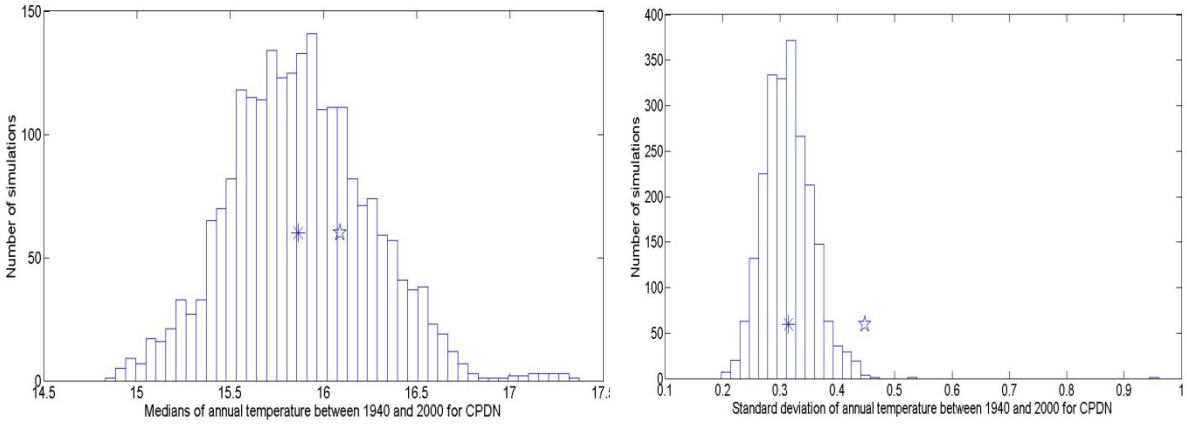

Figure 7 Histogram of the median of simulated (CPDN) annual temperature (°C) for the period between 1940 and 2000. Comparison of median of observed data (AWAP) as indicated with the open star and the median of all the simulations during the same period, indicated by an asterisk .

1009

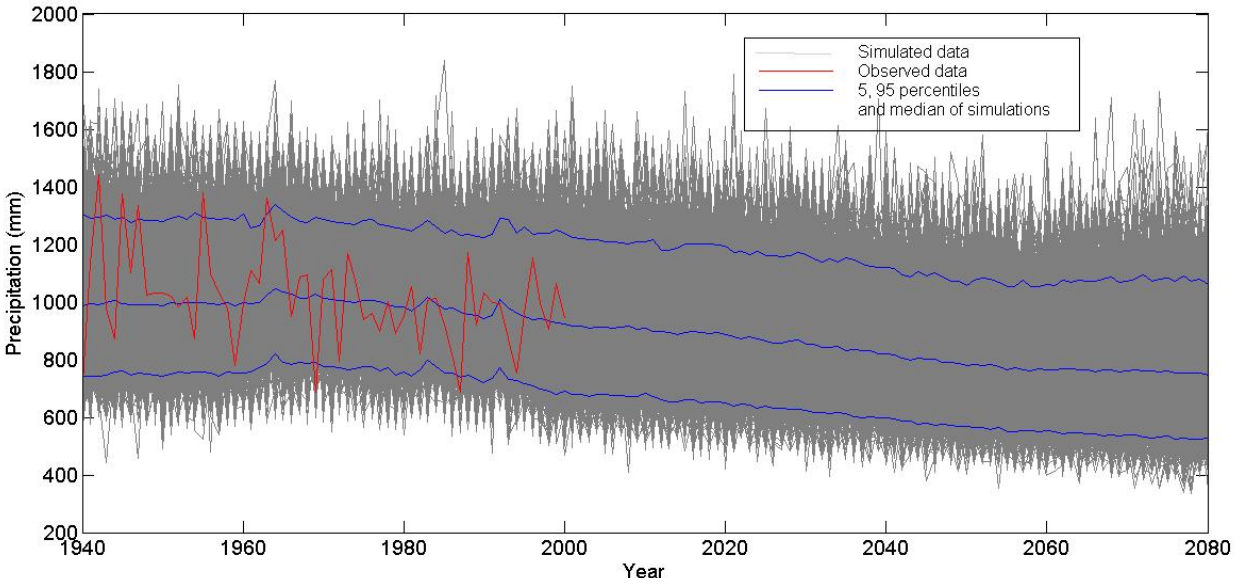

1010

1011 **Figure 8** Bias corrected annual precipitation over Donnelly River at Strickland. Grey lines
1012 represent the 2500 simulations of bias corrected precipitation from CPDN project. 95th, 5th
1013 percentiles and median of the simulations are presented as blue lines and AWAP annual
1014 precipitation is plotted with a red line. The bias correction was developed over the observed
1015 period 1961-1992

1016

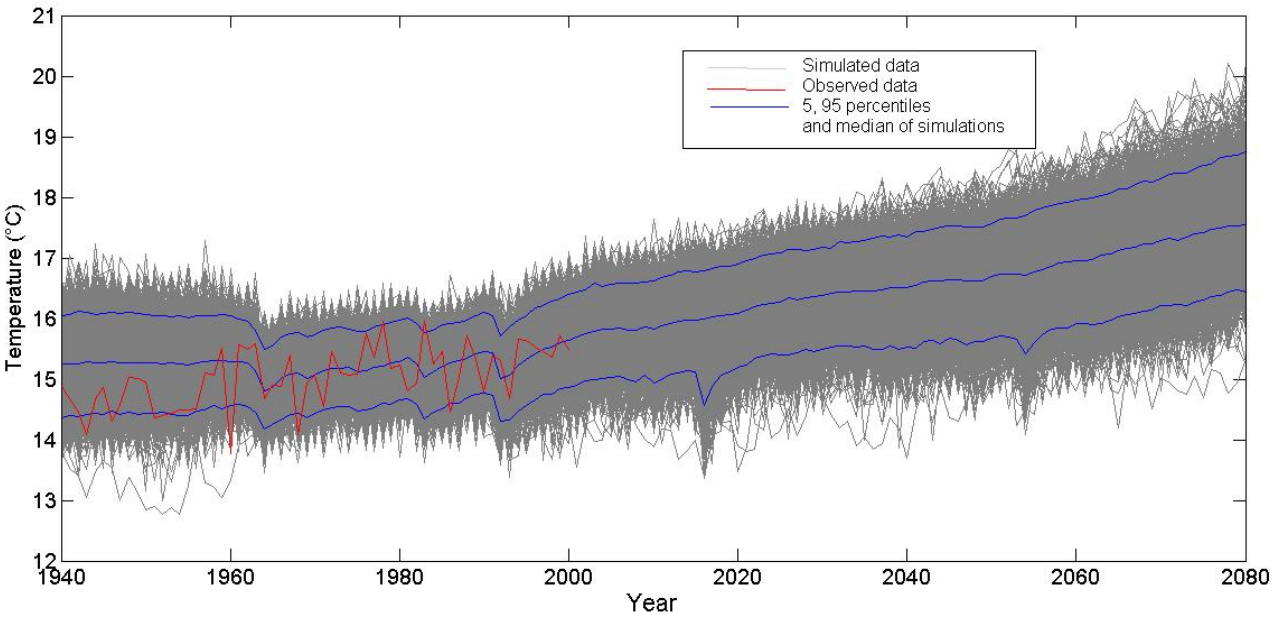

1017

1018 **Figure 9** Bias corrected annual temperature over Donnelly River at Strickland. Grey lines
1019 represent the 2500 simulations of bias corrected temperature from CPDN project. 95th, 5th
1020 percentiles and median of the simulations are presented as blue lines and AWAP annual
1021 temperature is plotted with red line The bias correction was developed over the observed
1022 period 1961-1992

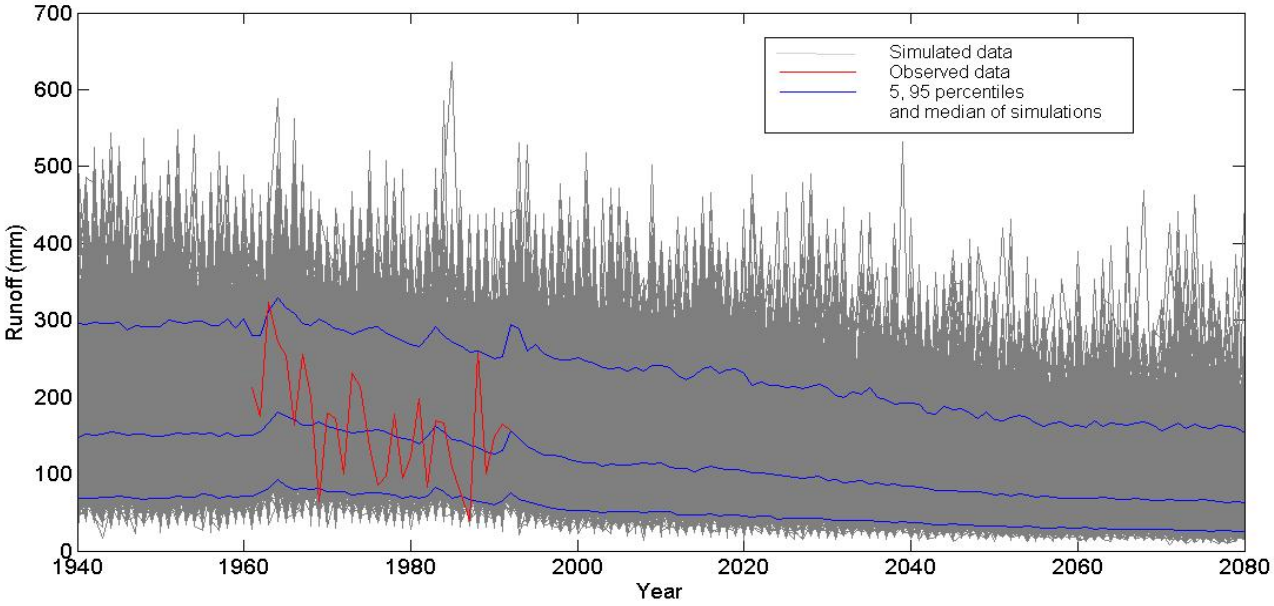

1023

1024 **Figure 10** Simulated annual runoff over Donnelly River at Strickland. Grey lines represent
1025 the 2500 simulations of runoff using PERM model run with bias corrected precipitation and
1026 temperature from CPDN. 95th, 5th percentiles and median of the simulations are presented
1027 as blue lines and observed runoff is plotted with a red line

1028

1029

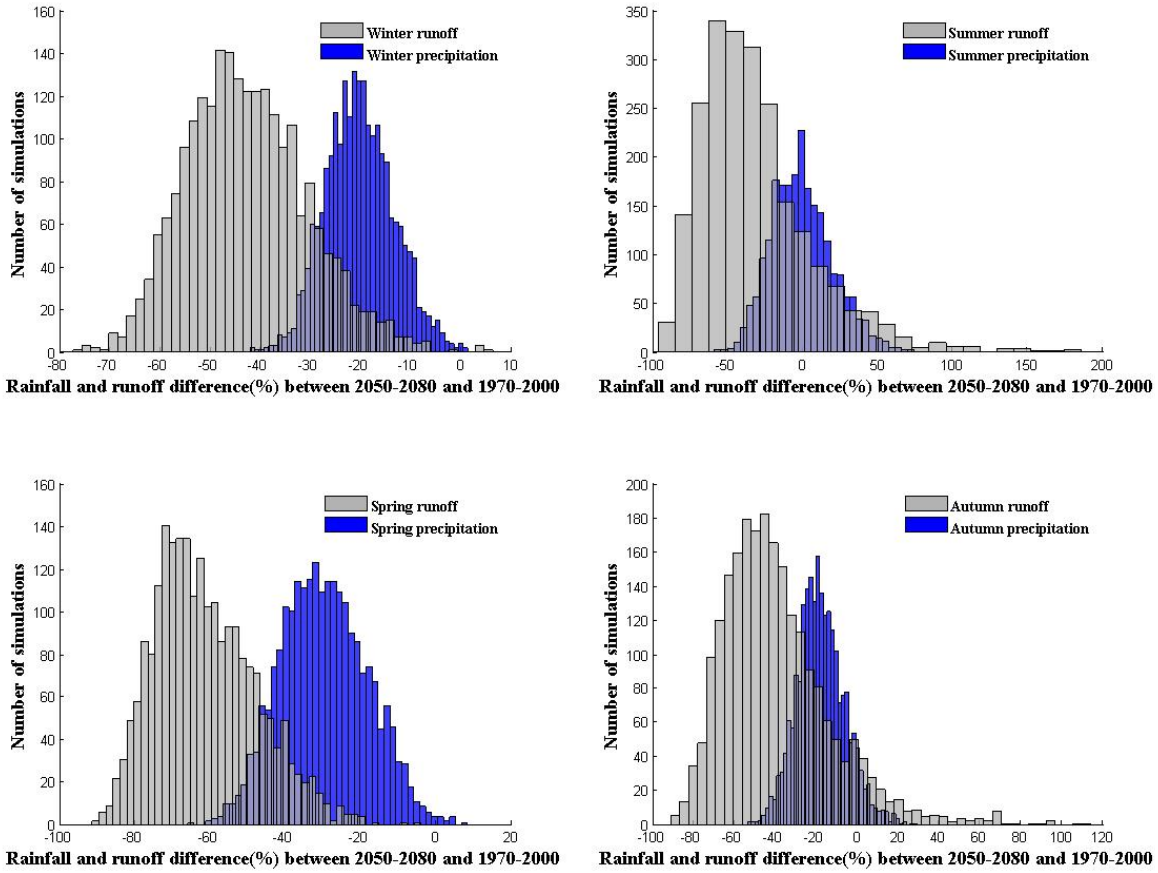

1030

1031 **Figure 11** Histograms of seasonal changes in precipitation and runoff over Donnelly River

1032 at Strickland

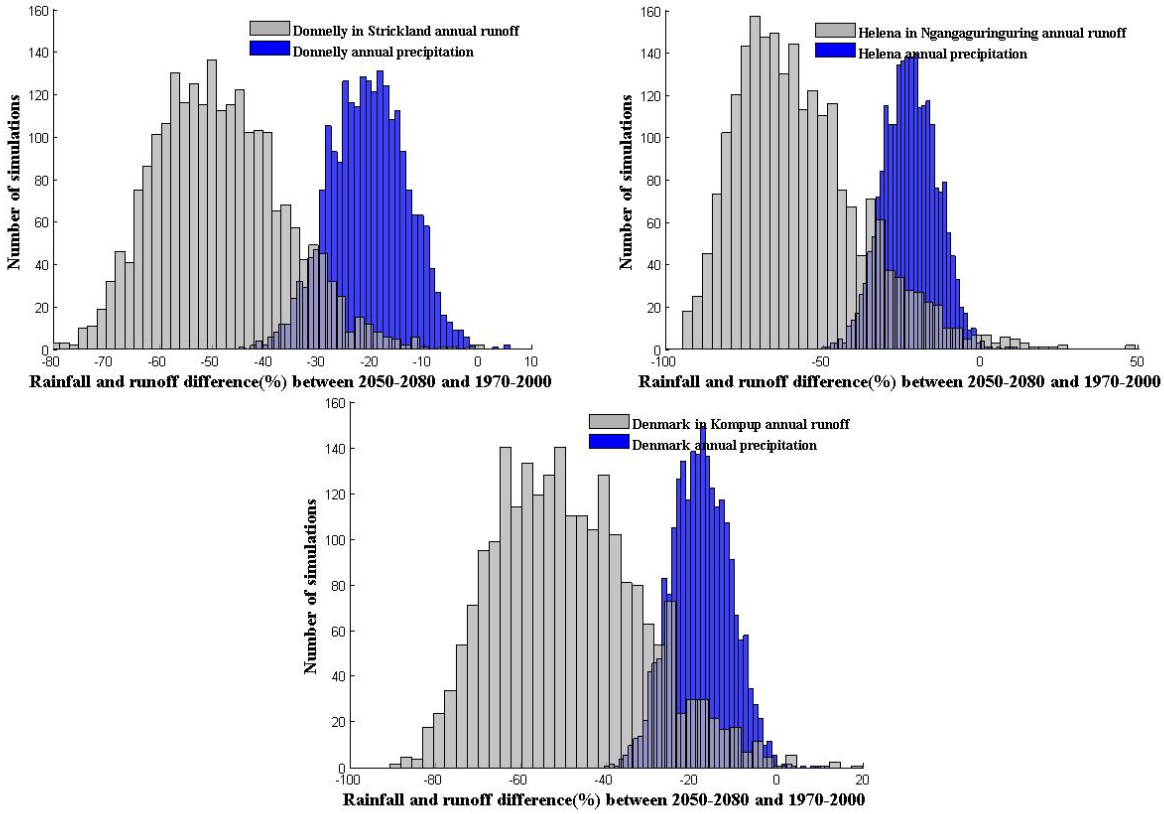

1033

1034 **Figure 12** Histograms of annual changes in precipitation and runoff in all of the catchments

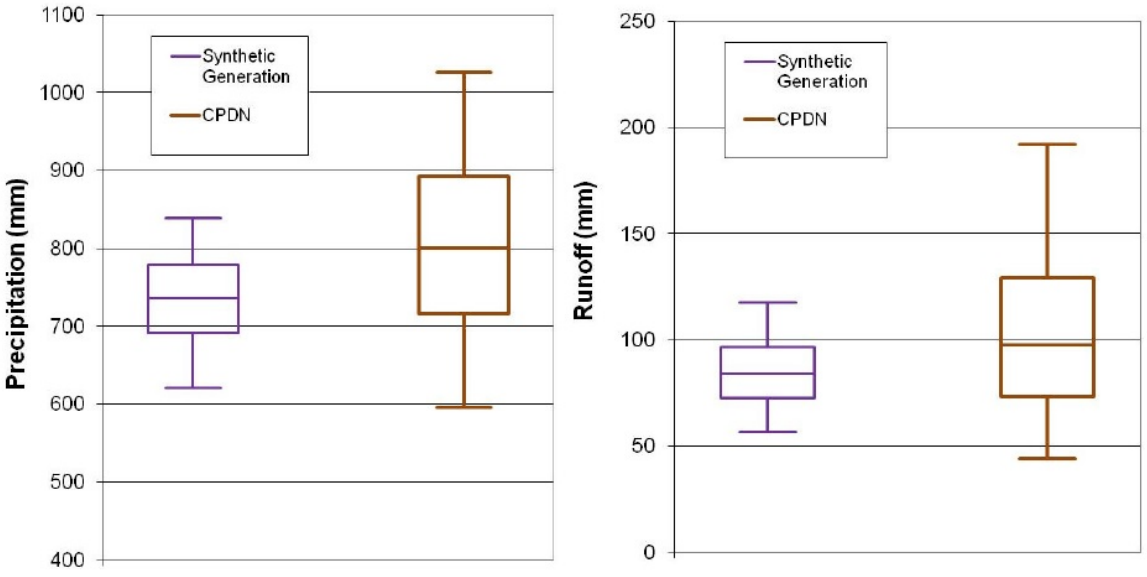

1035

1036 **Figure 13** Boxplot of uncertainties in precipitation and runoff using CPDN data and

1037 stochastic generation, in the Donnelly River at Strickland for the period 2035 - 2064

1038

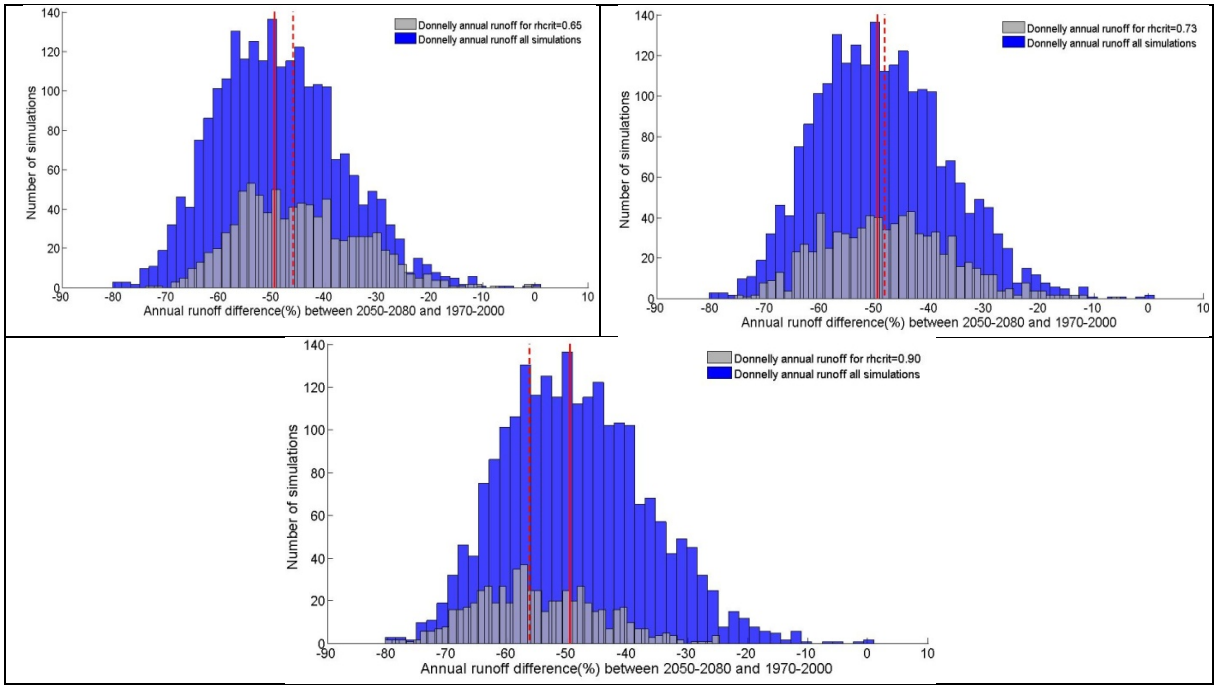

Figure 14 Histograms of annual changes in runoff considering all the simulations of CPDN and the groups of simulations with different perturbations of the parameter *rhcrit*. Red line represents the median of the whole ensemble and dotted red line the median of the simulations for a particular perturbation of *rhcrit*